

Ventral tegmental area GABA, glutamate, and glutamate-GABA neurons are heterogeneous in their electrophysiological and pharmacological properties

Jorge Miranda-Barrientos¹  | Ian Chambers¹ | Smriti Mongia¹ | Bing Liu¹ | Hui-Ling Wang¹ | Gabriel E. Mateo-Semidey¹ | Elyssa B. Margolis² | Shiliang Zhang³ | Marisela Morales¹

¹Integrative Neuroscience Research Branch, National Institute on Drug Abuse, Baltimore, MD, USA

²UCSF Weill Institute for Neurosciences, Department of Neurology, University of California, San Francisco, CA, USA

³Confocal and Electron Microscopy Core, National Institute on Drug Abuse, Baltimore, MD, USA

Correspondence

Marisela Morales, Integrative Neuroscience Research Branch, National Institute on Drug Abuse, 251 Bayview Blvd., Baltimore, Maryland 21224, USA.
Email: MMORALES@intra.nida.nih.gov

Funding information

NIH, Grant/Award Number: R01DA042025; Intramural research program NIH

A Commentary on this Article is available here: <https://doi.org/10.1111/ejn.15268>

Abstract

The ventral tegmental area (VTA) contains dopamine neurons intermixed with GABA-releasing (expressing vesicular GABA transporter, VGAT), glutamate-releasing (expressing vesicular glutamate transporter 2, VGLUT2), and glutamate-GABA co-releasing (co-expressing VGLUT2 and VGAT) neurons. By delivering INTRSECT viral vectors into the VTA of double *vglut2-Cre/vgat-Flp* transgenic mice, we targeted specific VTA cell populations for ex vivo recordings. We found that VGLUT2⁺ VGAT⁻ and VGLUT2⁺ VGAT⁺ neurons on average had relatively hyperpolarized resting membrane potential, greater rheobase, and lower spontaneous firing frequency compared to VGLUT2⁻ VGAT⁺ neurons, suggesting that VTA glutamate-releasing and glutamate-GABA co-releasing neurons require stronger excitatory drive to fire than GABA-releasing neurons. In addition, we detected expression of *Oprm1* mRNA (encoding μ opioid receptors, MOR) in VGLUT2⁺ VGAT⁻ and VGLUT2⁻ VGAT⁺ neurons, and that the MOR agonist DAMGO hyperpolarized neurons with these phenotypes. Collectively, we demonstrate the utility of the double transgenic mouse to access VTA glutamate, glutamate-GABA, and GABA neurons to determine their electrophysiological properties.

Significant statement: Some physiological properties of VTA glutamate-releasing and glutamate-GABA co-releasing neurons are distinct from those of VTA GABA-releasing neurons. μ -opioid receptor activation hyperpolarizes some VTA glutamate-releasing and some GABA-releasing neurons.

Abbreviations: 4-AP, 4-Aminopyridine; AAV, Adenos associated virus; ACSF, Artificial cerebrospinal fluid; AP, Action potential; A/P, Anterior/posterior; CV, Coefficient of variation; DAMGO, D-Ala², N-Me-Phe⁴, Gly⁵-ol]-Enkephalin; D/V, Doral/ventral; EGTA, Ethylene Glycol Tetraacetic Acid; eYFP, Enhanced yellow fluorescent protein; GABA, Gamma-aminobutyric acid; GAD, Glutamate decarboxylase; GFP, Green fluorescent protein; HCN1-4, Hyperpolarization-activated cyclic nucleotide-gated channel; HEPES, 4-(2-Hydroxyethyl)piperazine-1-ethanesulfonic acid, N-(2-Hydroxyethyl)piperazine-N'-(2-ethanesulfonic acid; Hz, Hertz; I_A , A-type K⁺ currents; I_h , Hyperpolarization-activated cation currents; INTRSECT, Intronic recombinase sites enabling combinatorial targeting; IRP, Intramural Research Program; ISI, Inter-spike intervals; JHU, Johns Hopkins University; LHA, Lateral hypothalamic area; M/L, Medial/lateral; MOR, μ -opioid receptors; mRNA, Messenger Ribonucleic acid; ms, Milliseconds; mV, Millivolts; NIDA, National Institute on Drug Abuse; NMDG, N-Methyl-D-glucamine; Oprm1, Opioid receptor mu 1; pA, Picoamperes; PB, Phosphate buffer; PFA, Paraformaldehyde.

Edited by: Yolanda Smith

© 2021 Federation of European Neuroscience Societies and John Wiley & Sons Ltd. This article has been contributed to by US Government employees and their work is in the public domain in the USA.

KEYWORDS

INTERSECT, MOR, mouse VTA, VGaT, VGluT2, VGluT2-VGaT

1 | INTRODUCTION

The ventral tegmental area (VTA) is a midbrain structure containing dopamine neurons (expressing tyrosine hydroxylase) that play a major role in motivated behaviors (Berridge, 2007; Bromberg-Martin et al., 2010; Wise, 2004). While the behavioral impact of VTA activity has classically been thought of as exclusively driven by dopaminergic output, the VTA contains multiple types of neurons, including neurons that release GABA (expressing the synthesis enzyme glutamate decarboxylase, GAD, and the vesicular GABA transporter, VGaT) and neurons that release glutamate (expressing vesicular glutamate transporter type 2, VGluT2) (Yamaguchi et al., 2007).

In addition, the VTA has neurons that co-release dopamine and glutamate, co-expressing TH and VGluT2 (Sulzer et al., 1998, Dal Bo et al., 2004, Stuber et al., 2010, Tecuapetla et al., 2010, Zhang et al. 2015), and neurons that co-express TH and VGaT that release GABA in the lateral habenula (Stamatakis et al., 2013). Moreover, some VTA dopamine neurons lacking GAD and VGaT co-release GABA (Tritsch et al., 2012). Recently, we demonstrated that the VTA contains neurons that express VGluT2 and VGaT (VGluT2⁺ VGaT⁺ neurons) and release both glutamate and GABA (Root et al., 2014); these neurons are intermixed with those that release glutamate without GABA (VGluT2⁺ VGaT⁻ neurons) or release GABA without glutamate (VGluT2⁻ VGaT⁺ neurons) (Root et al., 2018).

The *ex vivo* electrophysiological properties of putative dopamine neurons in the VTA have been investigated for decades; the identification of dopaminergic VTA neurons has been achieved by post hoc immunocytochemical detection of tyrosine hydroxylase (TH) in rat (Margolis et al., 2006) or by *in vivo* labeling in transgenic mice (Khaliq & Bean, 2010; Sawamoto et al., 2001). Characterization of VTA GABA neurons in *ex vivo* recordings has been achieved by GAD protein and mRNA detection in recorded neurons in rat (Margolis et al., 2012) or by *in vivo* labeling in transgenic mice with constitutive or viral vector-induced expression of green fluorescent protein (GFP) under the control of the GAD2 (Tan et al., 2012) or VGaT (van Zessen et al., 2012) promoters. *Ex vivo* recordings of VTA glutamate neurons have been made in mice that constitutively express GFP under the control of the VGluT2 promoter (Hnasko et al., 2012). Importantly, these studies did not differentiate neurons that co-release glutamate and GABA (VGluT2⁺ VGaT⁺) from those that are only glutamate-releasing (VGluT2⁺ VGaT⁻) or GABA-releasing (VGluT2⁻ VGaT⁺), raising the possibility that some of the overlapping physiological properties reported

in these groups specifically belong to the co-releasing population of neurons.

Single recombinase expressing transgenic mice had been used for the *in vivo* tagging of the entire populations of VTA neurons expressing either VGluT2 or VGaT, but these transgenic lines are not suitable for the selective tagging of VGluT2⁺ VGaT⁺, VGluT2⁺ VGaT⁻, or VGluT2⁻ VGaT⁺ neurons. To overcome this limitation, we recently generated a double *vglut2-Cre/vgat-Flp* transgenic mouse (Root et al., 2020). By injecting INTRSECT adeno associated viral (AAV) vectors (Fenno et al., 2014) into the VTA of *vglut2-Cre/vgat-Flp* transgenic mice, we induced expression of enhanced YFP (eYFP) in these different classes of VTA neurons. Using *ex vivo* recording, we found that some electrophysiological properties do vary across these classes of VTA neurons, and determined that not only VGluT2⁻ VGaT⁺ neurons, but also VGluT2⁺ VGaT⁻ neurons, are postsynaptically inhibited by MOR activation.

2 | MATERIALS AND METHODS

2.1 | Experimental subjects

Both male and female mice were used in this study. The *vglut2-IRES::Cre* mice (JAX # 016963) and *vgat::FlpO* mice (JAX # 031331; Daigle et al., 2018) were crossed to produce a *vglut2-IRES::Cre/vgat::FlpO* mice. Animals were housed in temperature- and humidity-controlled facilities under a 12 hr light/dark cycle with dawn at 0,700 hr and ad libitum chow and water prior to the start of experimental procedures. Mice were 2–3 months of age at the start of the experiment. Experiments were conducted in accordance with the USPHS Guide for the Care and Use of Laboratory Animals and approved by the Animal Care and Use Committee of the National Institute on Drug Abuse Intramural Research Program.

2.2 | Surgery and virus injections

Mice were anesthetized with isoflurane (2%–4% induction; 1% maintenance) and secured to a stereotaxic frame. After exposing the top of the skull, the mouse's head was leveled to ensure the skull was flat. One of the following three viruses were injected into the VTA (0.3 μ l; AP: -3.1 to -3.3, ML: \pm 0.0, DV: -4.3 to -4.4) to label the different classes of VTA neurons: (1) AAV5-Hsyn-CON-FON-eYFP to label VGluT2⁺ VGaT⁺ neurons, (2) AAV5-Hsyn-CON-FOFF-eYFP to label VGluT2⁺

VGaT⁻ neurons or (3) AAV5-Hsyn-COFF-FON-eYFP to label VGluT2⁻ VGaT⁺ neurons. Injections were made using a Micro4 controller and UltraMicroPump along with 10 μ l Nanofil syringes equipped with 35-gauge needles (WPI Inc., Sarasota, FL). Syringes were left in place for 10 min following injections to minimize diffusion. Following surgery, mice recovered on a warm heating pad before being transferred back to the vivarium home cage. During the following three days, mice were given the analgesic meloxicam (2 mg/kg) once a day to prevent post-surgical discomfort. Mice remained in the colony for 6–8 weeks to allow for virus expression for RNAscope experiments and electrophysiology experiments.

2.3 | Combination of RNAscope in situ hybridization and immunolabeling

Tissue preparation: Wild-type or Virus injected *vglut2-IRES::Cre/vgat::FlpO* mice were anesthetized with chloral hydrate (0.5 ml/kg) and perfused transcardially with 4% (w/v) paraformaldehyde (PFA) in 0.1 M phosphate buffer (PB), pH 7.3. Brains were left in 4% PFA for 2 hr and transferred to 18% sucrose in PB overnight at 4°C. The detection of transcripts encoding VGluT2 mRNA, VGaT mRNA, and Oprm1 mRNA was performed using RNAscope, and TH protein detection with immunohistochemistry. Coronal free-floating sections (wild-type mouse, VTA, 16 μ m) were incubated for 2 hr at 30°C with Mouse anti-TH antibody (1:1,000, MAB318, Millipore, Burlington, MA) in DEPC-treated phosphate buffer (PB) with 0.5% Triton X-100 supplemented with RNasin (Promega, Madison, WI). Sections were rinsed 3 \times 10 min with DEPC-treated PB, and incubated with secondary Donkey anti-Mouse Alexa Fluor 750 (1:100, ab175738, abcam, Cambridge, MA) for 1 hr at 30°C. Sections were rinsed with DEPC-treated PB and then were mounted onto Fisher SuperFrost slides and dried overnight at 60°C. RNAscope in situ hybridization processing was completed according to the manufacturer's instructions (Advanced Cell Diagnostics, Newark, CA). Briefly, sections were treated with heat and protease digestion followed by hybridization with a mixture containing target probes to mouse VGluT2 (319,171), VGaT (319191-C3), and Oprm1 (489311-C2). Additional sections were hybridized with the bacterial gene DapB as a negative control, which did not exhibit fluorescent labeling. VGluT2 was detected by Atto 550, VGaT was detected by Alexa 488, and Oprm1 was detected by Atto 647. GFP immunolabeling and detection of mRNA for VGluT2 and VGaT were performed as described above. VTA coronal free-floating sections (*vglut2-Cre / vgat-FlpO* mouse, 16 μ m in thickness) were processed for immunodetection of Mouse anti-GFP antibody (1:500, 632,381, Takara Bio USA, Inc. Mountain View, CA) and incubated with secondary Donkey anti-Mouse Alexa Fluor 488 (1:100, 715–545–151, Jackson ImmunoResearch, West Grove, PA), after processing

by RNAscope in situ hybridization, VGluT2 was detected by Atto 550, VGaT was detected by Atto 647. RNAscope in situ hybridization sections were viewed, analyzed, and photographed with an Olympus FV1000 confocal microscope or a Keyence BZ-X800 microscope. Negative control hybridizations showed negligible fluorophore expression. Neurons were counted when the stained cell was at least 5 μ m in diameter. Pictures were adjusted to match contrast and brightness by using Adobe Photoshop (Adobe Systems). The number of mice ($n = 3$ /group; 13–16 sections/mouse) utilized was selected based on previous studies in our lab using radioactive detection of VGluT2 mRNA from rat VTA neurons.

2.4 | Patch-clamp recordings

Six to eight weeks after virus injection, mice were anesthetized with isoflurane, decapitated, and the brains were quickly removed and placed in ice-cold artificial cerebrospinal fluid (ACSF), saturated with 95% O₂ and 5% CO₂, and modified to contain (in mM): 92 NMDG, 20 HEPES, 25 glucose, 30 NaHCO₃, 1.2 NaH₂PO₄, 2.5 KCl, 5 sodium ascorbate, 3 sodium pyruvate, 2 thiourea, 10 MgSO₄, 0.5 CaCl₂. Brains were sectioned through the VTA in horizontal slices (200 μ m thick) using a VT-1200 vibratome (Leica, Nussloch, Germany). The slices were placed in a holding chamber filled with the same solution but held at 32°C. After 10–15 min, slices were transferred to a holding chamber containing room temperature ACSF modified to contain (in mM): 92 NaCl, 20 HEPES, 25 glucose, 30 NaHCO₃, 1.2 NaH₂PO₄, 2.5 KCl, 5 sodium ascorbate, 3 sodium pyruvate, 2 thiourea, 1 MgSO₄, 2 CaCl₂. For recordings, slices were transferred to a chamber and superfused with 32°C ACSF containing (in mM): 125 NaCl, 2.5 KCl, 1.25 NaH₂PO₄, 1 MgCl₂, 2.4 CaCl₂, 26 NaHCO₃, and 11 glucose. Electrodes (2–4 M Ω) were backfilled with internal solution containing (in mM): 120 potassium gluconate, 8.0 NaCl, 1.0 MgCl₂, 10 HEPES, 2.0 Mg-ATP, 0.3 Na₂-GTP, 10 ditris-phosphocreatine, 0.2 EGTA and 0.2% biocytin (pH 7.2; 275–290 mOsm). Cells were visualized on an upright microscope using infrared and differential interference contrast video microscopy. Whole-cell voltage clamp and current clamp recordings were made using a MultiClamp 700B amplifier (2 kHz low-pass Bessel filter and 10 kHz digitization) with pClamp 10.3 software (Molecular Devices, Sunnyvale, CA). Firing rate was determined in cell attached mode 2–4 min after achieving a G Ω seal (to decrease the influence of potassium exposure from the recording pipette) for at least 60 s of continuous activity. Membrane potential and AP properties were measured in current clamp $I = 0$ within the first 5 min after gaining whole cell access. AP threshold was determined at the voltage point where the rate of the voltage change was greater than 5 mV/ms. AP duration was measured from AP threshold to the time when the descending voltage crossed the voltage

level of the AP threshold. AP amplitude was determined by obtaining the difference between the AP threshold and its positive peak. I_h was measured under voltage clamp mode holding at -60 mV and stepping to -120 , -100 , and -80 mV for 1,000 ms. I_A was measured in voltage clamp using a two step protocol. The first step consisted of a 500 ms hyperpolarization from holding potential of -60 mV to -120 mV, followed by increasing depolarizing steps from -100 mV to 30 mV in 10 mV increments for 1,000 ms. The second step was a depolarization from holding potential of -60 mV to -40 mV followed by depolarizing steps from -100 mV to 30 mV in 10 mV increments for 1,000 ms. I_A was calculated by subtracting the currents generated by the second protocol from the currents generated by the first protocol. In the current clamp recordings where I_A was blocked by 4-AP, an hyperpolarizing current was injected to maintain the membrane potential before the addition of 4-AP, and CNQX was applied to prevent increased AP firing due to an increase in glutamatergic transmission. Responses to the activation of MOR by DAMGO were measured under current clamp by determining the difference in membrane potential during baseline (5 min) and the membrane potential at steady-state (5 min) after adding DAMGO. A neuron was classified as responsive to DAMGO if the difference in membrane potential was greater than two millivolts.

2.5 | Classification of firing properties

To determine the firing properties and excitability of VTA neurons, input / output curves in response to depolarizing current steps of 500 ms duration from 0–150 pA were collected. The latency to initiate AP firing, number of APs fired during each current injection, frequency of AP firing, interspike intervals (ISIs), and the distribution over time of each AP fired during each current step were quantified. Neurons with latencies to initiate AP firing over 350 ms in response to the first two current injections able to initiate AP firing were considered long latency neurons. Neurons that underwent depolarization block within 300 ms of the initiation of current injections below 100 pA were considered depolarization block neurons. Neurons that maintained AP firing throughout a 500 ms current injection larger than 100 pA were considered continuous firing. If the ISIs of a neuron with continuous firing increased more than 50% during the first nine ISIs during the maximum current injection, the neuron was considered to have adaptation.

2.6 | Cluster analysis

Cluster analysis was performed on the data from 131 VTA neurons using 21 electrophysiological parameters that include: membrane potential, membrane capacitance,

membrane resistance, time constant, tonic firing frequency, coefficient of variation of ISI, I_h amplitude, rheobase, AP threshold, difference between resting membrane potential and AP threshold, AP amplitude, AP duration, after hyperpolarization amplitude, after hyperpolarization duration, after hyperpolarization minimum, latency to fire at rheobase, number of APs fired at rheobase, number of APs fired during rebound firing, greatest number of APs in response to depolarization, current to induce greatest number of APs, highest firing frequency. Parameter values were normalized to prevent over representation of a specific parameter during clustering. Analysis was performed in R-studio software using K-means method and Euclidean distance. The result of the clustering was plotted as a dendrogram. The principal components that best separated the clusters were identified and statistical comparisons between clusters were performed.

2.7 | Localization of biocytin filled neurons and TH immunostaining of recorded cells

After patch-clamp recordings, the recording electrode was carefully withdrawn, and the slices were fixed overnight at 4 °C in 4% paraformaldehyde in phosphate buffer solution (PBS). After thorough rinsing with PBS and permeabilization with 0.3% Triton X-100 (Sigma-Aldrich), the slices were incubated overnight with streptavidin-CY3 (1:50, 438,315, Invitrogen, USA) or streptavidin-CY5 (1:50, 438,315, Invitrogen, USA). Slices were then rinsed with PBS and mounted onto Fisher SuperFrost slides for visualization in an Olympus FV1000 confocal microscope. Low magnification (10 \times) was used to localize the recorded neurons, confirming that they were within the boundaries of the VTA. Slices that contained a labeled neuron were transferred back to a PBS solution and after additional permeabilization with 0.3% Triton X-100, they were incubated overnight with a mouse anti-TH antibody (1:100, MAB318, Millipore, Burlington, MA). Sections were rinsed with PBS and then incubated with secondary Donkey anti-Mouse Alexa Fluor 405 (1:100, ab175658, abcam, Cambridge, MA) for 1 hr at 30°C. Sections were rinsed with PBS and then mounted onto Fisher SuperFrost slides and visualized using higher magnification (40 \times) on an Olympus FV1000 confocal microscope.

2.8 | Statistical analysis

Data in the figures are presented as mean \pm SEM. Student's *t*-test, one-way ANOVA with Tukey's or Dunnett's *post-hoc* test, and two-way ANOVA with Bonferroni's *post-hoc* test were performed to compare groups of neurons (Prism 5.0 software). $p < 0.05$ was required for significance.

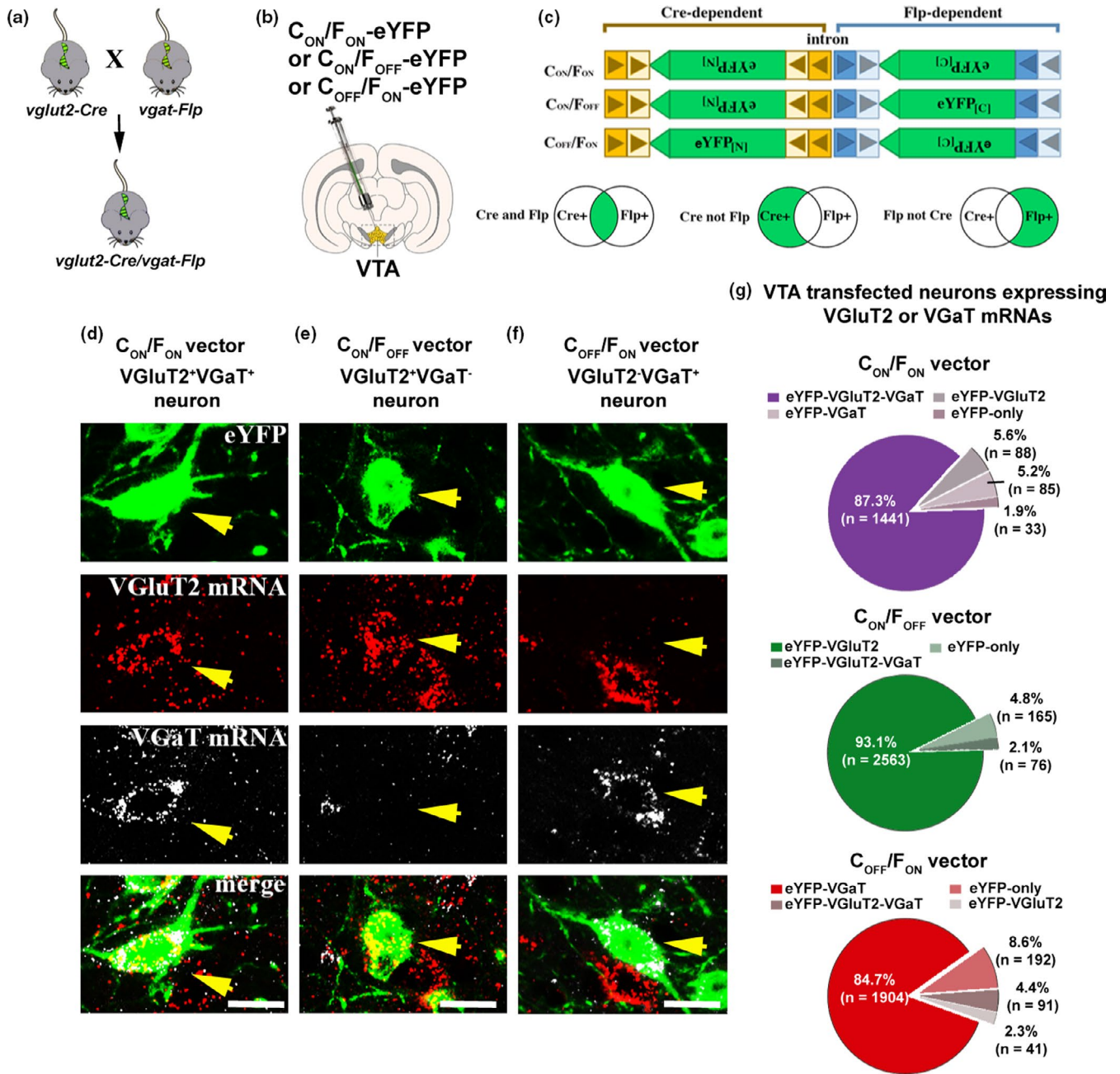


FIGURE 1 Selective targeting of VTA VGluT2⁺ VGaT⁺, VGluT2⁺ VGaT⁻, and VGluT2⁻ VGaT⁺ neurons. (a-c) Crossing *vglut2-Cre* and *vgat-Flp* mice to generate *vglut2-Cre/vgat-Flp* mice, and intra-VTA injections of INTRSECT AAV-C_{ON}/F_{ON}-eYFP to target VGluT2⁺ VGaT⁺ neurons, AAV-C_{ON}/F_{OFF}-eYFP to target VGluT2⁺ VGaT⁻ neurons or AAV-C_{OFF}/F_{ON}-eYFP to target VGluT2⁻ VGaT⁺ neurons. (d) Co-expression of VGluT2 mRNA and VGaT mRNA in VTA VGluT2⁺ VGaT⁺ eYFP neuron. Scale bar = 20 μM. (e) VGluT2 mRNA without VGaT mRNA in VTA VGluT2⁺ VGaT⁻ eYFP neuron. Scale bar = 20 μM. (f) VGaT mRNA without VGluT2 mRNA in VTA VGluT2⁻ VGaT⁺ eYFP neuron. Scale bar = 20 μM. (g) Percentage of VTA transfected neurons co-expressing VGluT2 mRNA or VGaT mRNA (n = 3 mice per group)

3 | RESULTS

3.1 | Selective targeting of VTA VGluT2⁺ VGaT⁺, VGluT2⁺ VGaT⁻, and VGluT2⁻ VGaT⁺ neurons

To tag VGluT2⁺ VGaT⁺, VGluT2⁺ VGaT⁻, and VGluT2⁻ VGaT⁺ neurons, we generated *vglut2-Cre/vgat-Flp* mice by

crossing *vglut2-Cre* mice with *vgat-Flp* mice (Figure 1a) and injected INTRSECT adeno associated viral (AAV) vectors into their VTA (Fenno et al., 2014). In different cohorts of *vglut2-Cre/vgat-Flp* mice, we injected AAV-C_{ON}/F_{ON}-eYFP vectors (requiring Cre and Flp recombinases for eYFP expression) to target VGluT2⁺ VGaT⁺ neurons; AAV-C_{ON}/F_{OFF}-eYFP vectors (requiring the presence of Cre recombinase and absence of Flp recombinase for eYFP expression)

to target VGluT2⁺ VGaT⁻ neurons; or AAV-C_{OFF}/F_{ON}-eYFP vectors (requiring the absence of Cre recombinase and presence of Flp recombinase for eYFP expression) to target VGluT2⁻ VGaT⁺ neurons (Figure 1b-c).

After confirming VTA neuronal expression of eYFP in each cohort of mice (Figure 1d-f), we examined the mRNA expression of VGluT2 or VGaT within eYFP expressing neurons (Figure D-F). In the VTA of mice locally injected with AAV-C_{ON}/F_{ON}-eYFP vectors (to tag VGluT2⁺ VGaT⁺ neurons) (Figure 1d), we found that within the total population of eYFP expressing neurons (1,647 neurons, three mice; Figure 1g), approximately 90% expressed both VGluT2 and VGaT mRNAs (87.3% ± 2.4%; 1,441/1,647), 6% expressed only VGluT2 mRNA (5.6% ± 1.6%; 88/1,647 neurons), close to 5% expressed only VGaT mRNA (5.2% ± 2.0%; 85/1,647, Figure 1g), and few lacked both VGluT2 and VGaT mRNAs (1.93% ± 0.35%; 33/1,647). In the VTA of mice locally injected with AAV-C_{ON}/F_{OFF}-eYFP vectors (to tag VGluT2⁺ VGaT⁻ neurons) (Figure 1e), we found that within the total population of eYFP neurons (2,804 neurons, 3 mice; Figure 1g) more than 90% expressed VGluT2 mRNA (93.1% ± 2.8%, 2,563/2,804), none expressed VGaT mRNA alone, very few expressed VGluT2 mRNA together with VGaT mRNA (2.1% ± 0.9%, 76/2,804), and a small number lacked both VGluT2 or VGaT mRNAs (4.8% ± 2.0%, 165/2,804). In the VTA of mice locally injected with AAV-C_{OFF}/F_{ON}-eYFP vectors (to label VGluT2⁻ VGaT⁺ neurons) (Figure 1f), we found that within the total population of eYFP neurons, close to 85% expressed VGaT mRNA (84.7% ± 2.1%, 1,904/2,228 neurons, three mice) (Figure 1f-g), rare cases expressed VGluT2 mRNA (2.3% ± 1.1%, 41/2,228 neurons) (Figure 1g), a small quantity had VGaT mRNA together with VGluT2 mRNA (4.4% ± 1.4%; 91/2,228 neurons) (Figure 1g), and less than 10% lacked both VGluT2 and VGaT mRNAs (8.6% ± 0.5%, 192/2,228 neurons) (Figure 1g). Collectively, these findings indicate that using *vglut2-Cre/vgat-Flp* mice in combination with the tested INTRSECT viral vectors for the selective tagging of the three classes of VTA neurons generates very few false positive classifications.

3.2 | Intrinsic properties of VTA VGluT2⁺ VGaT⁺, VGluT2⁺ VGaT⁻, and VGluT2⁻ VGaT⁺ neurons

Next, we determined the spontaneous AP activity of the three classes of neurons with cell attached recordings in acute horizontal brain slices. We detected spontaneous activity in 46.2% of the VGluT2⁺ VGaT⁺ neurons (24/52 neurons, 28 mice), 49.0% of the VGluT2⁺ VGaT⁻ neurons (24/49 neurons, 27 mice), and 70.7% of the VGluT2⁻ VGaT⁺ neurons (29/41 neurons, 19 mice) (Figure 2c). Among the spontaneously active neurons (77 neurons), we found that the mean firing frequency was lower in VGluT2⁺ VGaT⁺ and VGluT2⁺ VGaT⁻ neurons compared to VGluT2⁻ VGaT⁺ neurons (3.4 ± 0.7 Hz for VGluT2⁺ VGaT⁺, *n* = 24 neurons, 20 mice; 3.5 ± 0.7 Hz for VGluT2⁺ VGaT⁻, *n* = 24 neurons, 18 mice; and 8.3 ± 2.1 Hz for VGluT2⁻ VGaT⁺, *n* = 29 neurons, 14 mice) (Figure 2b,d). Together these findings indicate that more VGluT2⁻ VGaT⁺ neurons fire spontaneously, and on average they fire faster, than VGluT2⁺ VGaT⁺ or VGluT2⁺ VGaT⁻ neurons. Next, we analyzed the extracellular AP durations from these neurons and found that VGluT2⁺ VGaT⁺ neurons have similar AP durations to VGluT2⁻ VGaT⁺ neurons, and both of these phenotypes on average have shorter AP durations than VGluT2⁺ VGaT⁻ neurons (1.3 ± 0.1 ms for VGluT2⁺ VGaT⁺, *n* = 24 neurons, 20 mice; 1.7 ± 0.1 ms for VGluT2⁺ VGaT⁻, *n* = 24 neurons, 18 mice; and 1.2 ± 0.1 ms for VGluT2⁻ VGaT⁺, *n* = 29 neurons, 14 mice) (Figure 2f,g). Because VTA neurons are known to have pacemaker activity as well as burst firing patterns, we also evaluated the regularity of firing. We analyzed the coefficient of variation (CV) of ISIs and found that VGluT2⁺ VGaT⁺ neurons had higher mean CVs of ISIs compared to VGluT2⁻ VGaT⁺ neurons (0.48 ± 0.06 for VGluT2⁺ VGaT⁺, 0.41 ± 0.06 for VGluT2⁺ VGaT⁻, and 0.37 ± 0.04 for VGluT2⁻ VGaT⁺). However, the differences in CVs were not significant (Figure 2e). These findings indicate that there are no clear differences in the regularity of spontaneous firing between VGluT2⁺ VGaT⁺, VGluT2⁺ VGaT⁻, and VGluT2⁻ VGaT⁺ neurons.

Next, using whole-cell recordings, we examined intrinsic electrophysiological properties of these three classes of VTA

FIGURE 2 Spontaneous firing activity in VTA VGluT2⁺ VGaT⁺, VGluT2⁺ VGaT⁻, and VGluT2⁻ VGaT⁺ neurons during ex vivo cell attached recordings. (a) Schematic representation of intra-VTA injections of vectors (AAV-C_{ON}/F_{ON}-eYFP, AAV-C_{ON}/F_{OFF}-eYFP and AAV-C_{OFF}/F_{ON}-eYFP) in *vglut2-Cre/vgat-Flp* mice. (b) Traces recorded in the cell attached configuration in horizontal slices from identified spontaneously active VTA neurons. (c) Proportion of VTA neurons spontaneously active versus quiescent. (d) Summary of spontaneous firing rates. VGluT2⁻ VGaT⁺ neurons had higher firing frequencies than VGluT2⁺ VGaT⁺ and VGluT2⁺ VGaT⁻ neurons. One-way ANOVA $F_{2,77} = 5.795$, $p = 0.046$; Tukey's *post hoc* test $*p < 0.05$. (e) There was no relationship between firing frequency and coefficient of variation (CV) of inter-spike intervals (ISIs) for these neuronal types. Inset, summary of CV of ISIs in VGluT2⁺ VGaT⁺, VGluT2⁺ VGaT⁻, and VGluT2⁻ VGaT⁺ neurons. Example traces (f) and summary (g) of extracellular AP durations. One-way ANOVA $F_{2,77} = 6.745$, $p = 0.0026$; Tukey's *post hoc* test $*p < 0.05$, $**p < 0.01$

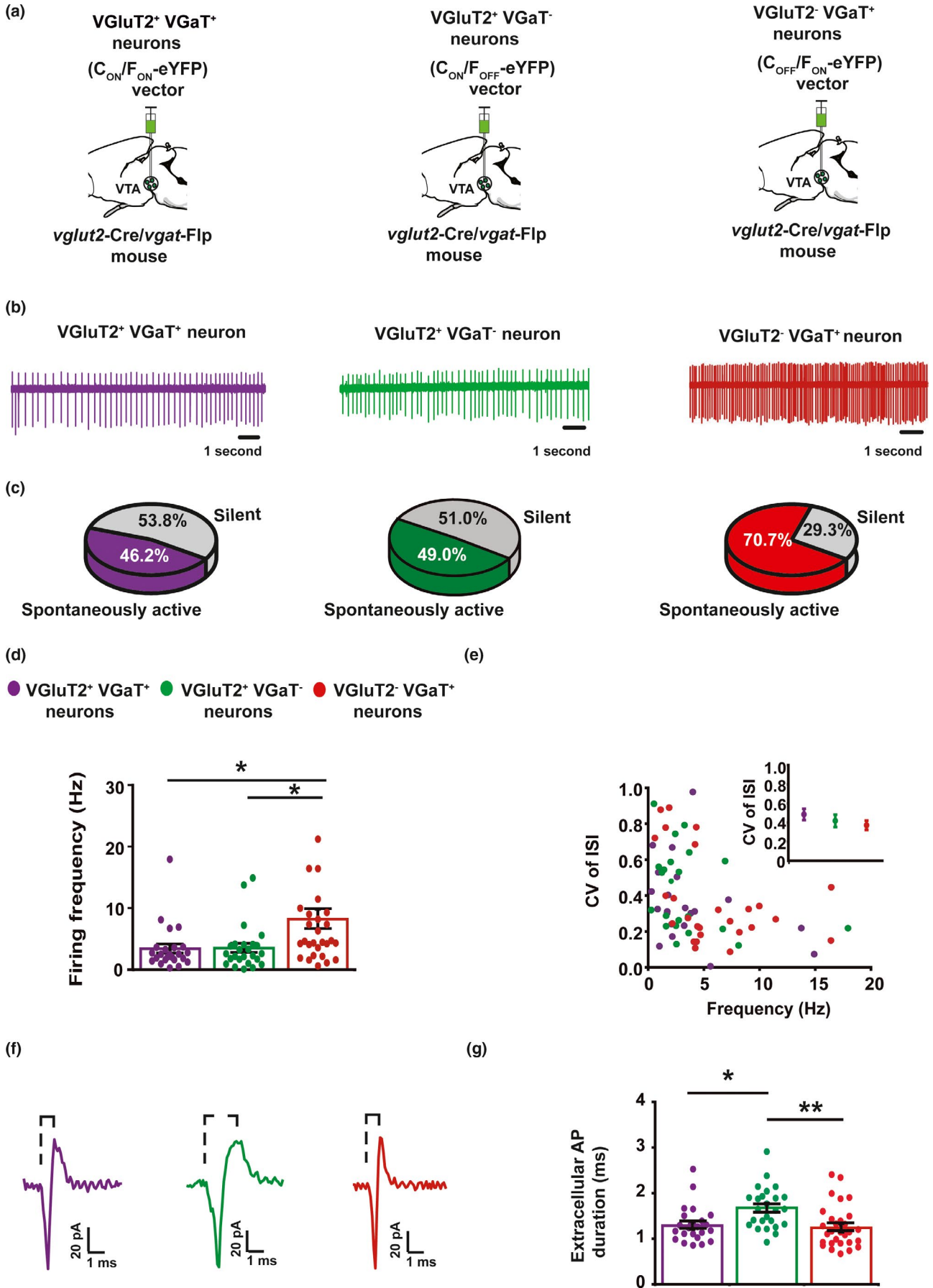


TABLE 1 Intrinsic membrane and action potential properties of VTA VGluT2⁺ VGaT⁺, VGluT2⁺ VGaT⁻, and VGluT2⁻ VGaT⁺ neurons

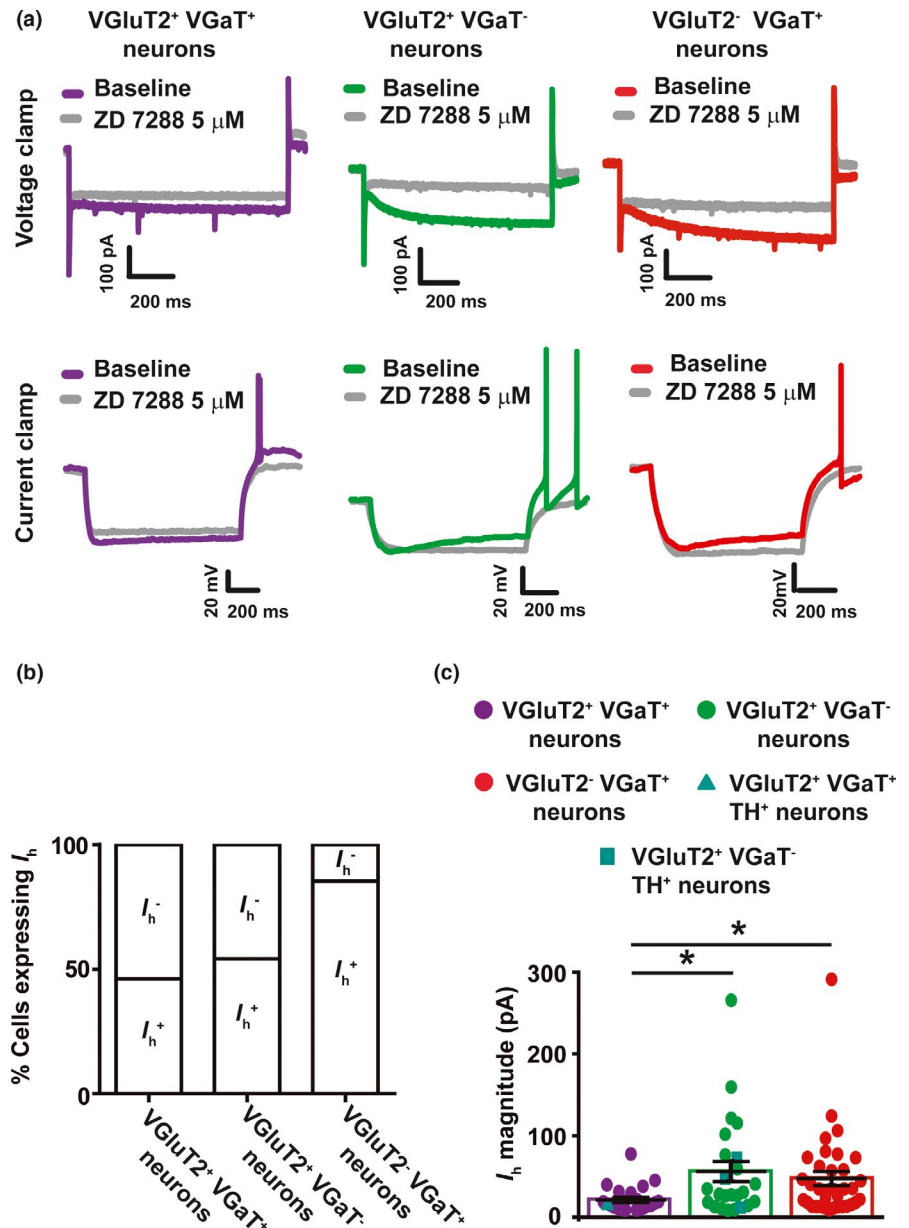
Class of VTA neuron	*Membrane potential (mV)	Membrane resistance (MOhms)	Capacitance (pF)	*Rheobase (pA)	AP Threshold (mV)	Gap (mV)	AP amplitude (mV)	*AP duration (ms)
VGluT2 ⁺ VGaT ⁺ (N = 52)	-68.0 ± 1.2	644.7 ± 68.4	30.9 ± 2.0	29.0 ± 5.5	-39.1 ± 0.5	28.8 ± 1.3	70.7 ± 1.3	2.2 ± 0.1
VGluT2 ⁺ VGaT ⁻ (N = 48)	-64.6 ± 0.9	655.7 ± 42.5	26.6 ± 1.3	37.3 ± 5.6	-36.7 ± 0.7	28.0 ± 1.0	69.7 ± 1.0	2.9 ± 0.2
VGluT2 ⁻ VGaT ⁺ (N = 41)	-59.6 ± 0.9	549.7 ± 53.7	30.6 ± 1.6	14.9 ± 2.9	-38.4 ± 0.8	21.1 ± 0.9	72.9 ± 1.6	1.8 ± 0.1

Note: Action potential (AP). Difference from membrane potential and AP threshold (Gap). Millivolts (mV). Megaohms (MOhms). Picoamperes (pA). Milliseconds (ms). Membrane potential: One-way ANOVA $F_{2,140} = 16.65$ $p < 0.0001$; Tukey's *post hoc* test *VGluT2⁺ VGaT⁺ versus VGluT2⁺ VGaT⁻ $p < 0.05$, **VGluT2⁺ VGaT⁻ versus VGluT2⁻ VGaT⁺ $p < 0.01$, ***VGluT2⁺ VGaT⁺ versus VGluT2⁻ VGaT⁺ $p < 0.001$. Rheobase: One-way ANOVA $F_{2,140} = 4.571$ $p = .0120$; Tukey's *post hoc* test **VGluT2⁺ VGaT⁻ versus VGluT2⁻ VGaT⁺ $p < 0.01$. Gap: One-way ANOVA $F_{2,130} = 12.37$ $p < 0.0001$; Tukey's *post hoc* test ***VGluT2⁺ VGaT⁺ versus VGluT2⁻ VGaT⁺ $p < 0.001$, ***VGluT2⁺ VGaT⁻ versus VGluT2⁻ VGaT⁺ $p < 0.0001$; Tukey's *post hoc* test **VGluT2⁺ VGaT⁺ versus VGluT2⁻ VGaT⁺ $p < 0.001$, ***VGluT2⁺ VGaT⁻ versus VGluT2⁻ VGaT⁺ $p < 0.001$.

neurons. We found that the resting membrane potential was -68.0 ± 1.2 mV for VGluT2⁺ VGaT⁺ neurons ($n = 52$ neurons, 27 mice), -64.6 ± 0.9 mV for VGluT2⁺ VGaT⁻ neurons ($n = 49$ neurons, 27 mice), and -59.6 ± 0.9 mV for VGluT2⁻ VGaT⁺ neurons ($n = 41$ neurons, 19 mice). We detected the greatest rheobase in VGluT2⁺ VGaT⁻ neurons (37.3 ± 5.6 pA, $n = 48$ neurons, 27 mice), followed by VGluT2⁺ VGaT⁺ neurons (29.0 ± 5.5 pA, $n = 52$ neurons, 28 mice), and the lowest rheobase in VGluT2⁻ VGaT⁺ neurons (14.9 ± 2.9 pA, $n = 41$, 19 mice) (Table 1). Collectively these findings indicate that VTA neurons expressing VGluT2, with or without VGaT, are less excitable than VTA neurons lacking VGluT2, and the VGluT2⁺ VGaT⁻ neurons are the least excitable among the 3 classes. No differences in membrane capacitance, membrane resistance, membrane time constant, or AP threshold were observed. However, in line with our cell attached data, we found that on average VGluT2⁺ VGaT⁻ neurons have longer duration APs than VGluT2⁺ VGaT⁺ and VGluT2⁻ VGaT⁺ neurons (2.2 ± 0.1 ms for VGluT2⁺ VGaT⁺, $n = 52$ neurons, mice; 2.9 ± 0.2 ms for VGluT2⁺ VGaT⁻, $n = 48$ neurons, 27 mice and 1.8 ± 0.1 ms for VGluT2⁻ VGaT⁺, $n = 41$ neurons, 19 mice) (Table 1).

Given that hyperpolarization-activated cation currents (I_h) are present in both dopamine and non-dopamine neurons (Hnasko et al., 2012; Jones & Kauer, 1999; Margolis et al., 2006, 2012), we tested the three classes of VTA neurons for I_h . We detected I_h in 46.2% of VGluT2⁺ VGaT⁺ neurons (24/52 neurons, 28 mice), 54.1% of VGluT2⁺ VGaT⁻ neurons (26/48 neurons from 24 mice), and 85.4% of VGluT2⁻ VGaT⁺ neurons (35/41 neurons, 18 mice) (Figure 3b). While there was a wide range of I_h magnitudes among each cell type, the mean I_h magnitude was smaller in VGluT2⁺ VGaT⁺ neurons compared to VGluT2⁺ VGaT⁻ neurons or VGluT2⁻ VGaT⁺ neurons (22.4 ± 3.2 pA for VGluT2⁺ VGaT⁺, 58.8 ± 11.0 pA for VGluT2⁺ VGaT⁻, and 48.6 ± 8.4 pA for VGluT2⁻ VGaT⁺) (Figure 3a,c). We also determined the extent to which the recorded neurons filled with biocytin expressed TH protein with post hoc immunohistochemistry, and from those neurons, the number that expressed I_h . From a total of 35 VGluT2⁺ VGaT⁺ neurons analyzed, only one expressed TH, and this neuron had an I_h of 17.1 pA (Figure 3c; 4A-C). Among 20 VGluT2⁺ VGaT⁻ neurons analyzed, 6 expressed TH (VGluT2⁺ VGaT⁻ TH⁺ neurons); three of these had an I_h (42.9 ± 17.5 pA) (Figures 3c and 4a-c). Of the 26 VGluT2⁻ VGaT⁺ analyzed neurons, none expressed TH (Figure 4a-b). We found that regardless of the neuronal cell type, the neurons with larger I_h magnitudes were located in the lateral VTA and those with low amplitudes were in the medial VTA. These findings support a VTA latero-medial neuronal topography among non-dopamine neurons, similar to that found among dopamine neurons.

FIGURE 3 I_h presence in VTA VGluT2⁺ VGaT⁺, VGluT2⁺ VGaT⁻, and VGluT2⁻ VGaT⁺ neurons. (a) Voltage clamp (top; step from -60 mV to -120 mV, 1 s duration) and current clamp (bottom; step from 0 pA to 50–100 pA to reach $V_m = -120$ mV) traces of I_h measurements in VTA neurons. I_h was blocked with ZD 7,288 (5 μ M; gray traces). (b) Proportion of each VTA neuronal types that expressed I_h . (c) Smaller mean I_h amplitude was observed in VGluT2⁺ VGaT⁺ neurons compared to VGluT2⁺ VGaT⁻ or VGluT2⁻ VGaT⁺ neurons. One-way ANOVA $F_{2,82} = 3.528$, $p = 0.034$, Tukey's *post hoc* test $*p < 0.05$



3.3 | Stimulated firing patterns of VTA VGluT2⁺ VGaT⁺, VGluT2⁺ VGaT⁻, and VGluT2⁻ VGaT⁺ neurons

We next examined the stimulated firing patterns of these three classes of neurons by inducing AP firing in current clamp with a series of depolarizing current steps (500 ms, 10–150 pA). We found that most VGluT2⁺ VGaT⁺ neurons (41/48 neurons, 24 mice) fired APs with short latency from initiation of the current pulse (149 ± 10 ms; Figure 5a-b,d). A small group of neurons responded to the injected current with delayed firing (7/48 neurons, 7 mice; 450 ± 9 ms; Figure 5a-b,d; 1/7 neuron expressed TH; Figure 5d), displaying a slow depolarizing ramp prior to the first AP (Figure 5a). We found that the rheobase was generally greater in VGluT2⁺ VGaT⁺ neurons with long latency (101.4 ± 24.8 pA Figure 5c) than in those

with short latency (17.8 ± 2.5 pA; Figure 5c). We observed that current injections below 100 pA produced depolarization block in some of the short latency neurons (14/41 neurons, eight mice; Figure 5d). Across all short latency VGluT2⁺ VGaT⁺ neurons (41 neurons), more than half of them fired APs continuously during the entire current injection (27/41 neurons, 18 mice; Figure 5d). Furthermore, many of these neurons also showed frequency adaptation (more evident at current injections above 100 pA; 18/27 neurons, 12 mice; Figure 5d), with the ISI increasing after each AP (Figure 6a), but others either lacked or had minimal frequency adaptation (9/27 neurons, seven mice; Figure 6a) which permitted higher sustained firing rates (38.7 ± 3.2 Hz in neurons with adaptation; 84.2 ± 5.7 Hz in neurons without adaptation). VGluT2⁺ VGaT⁻ neurons were similar to VGluT2⁺ VGaT⁺ neurons, with short latency AP firing in response to injected current

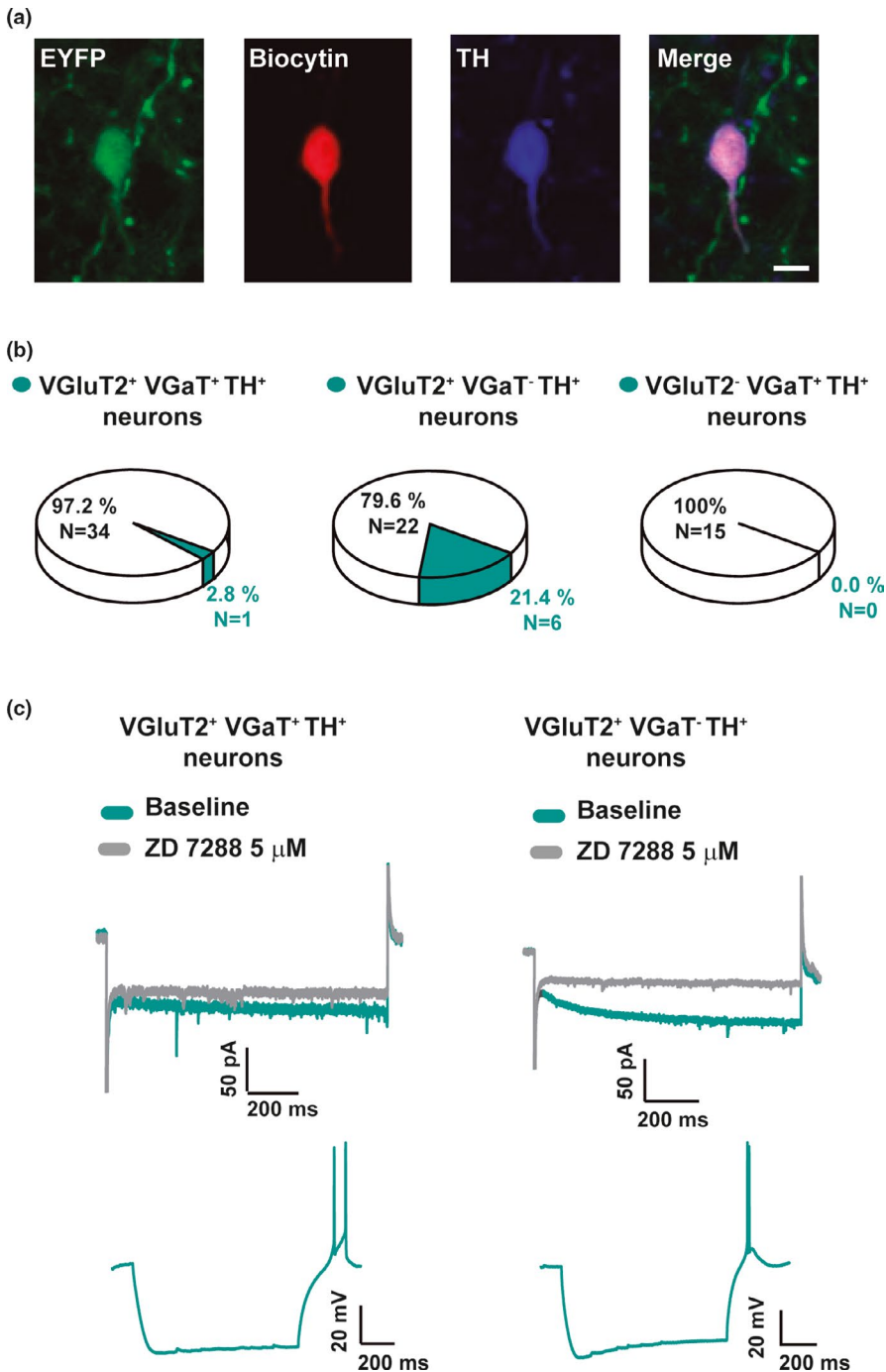
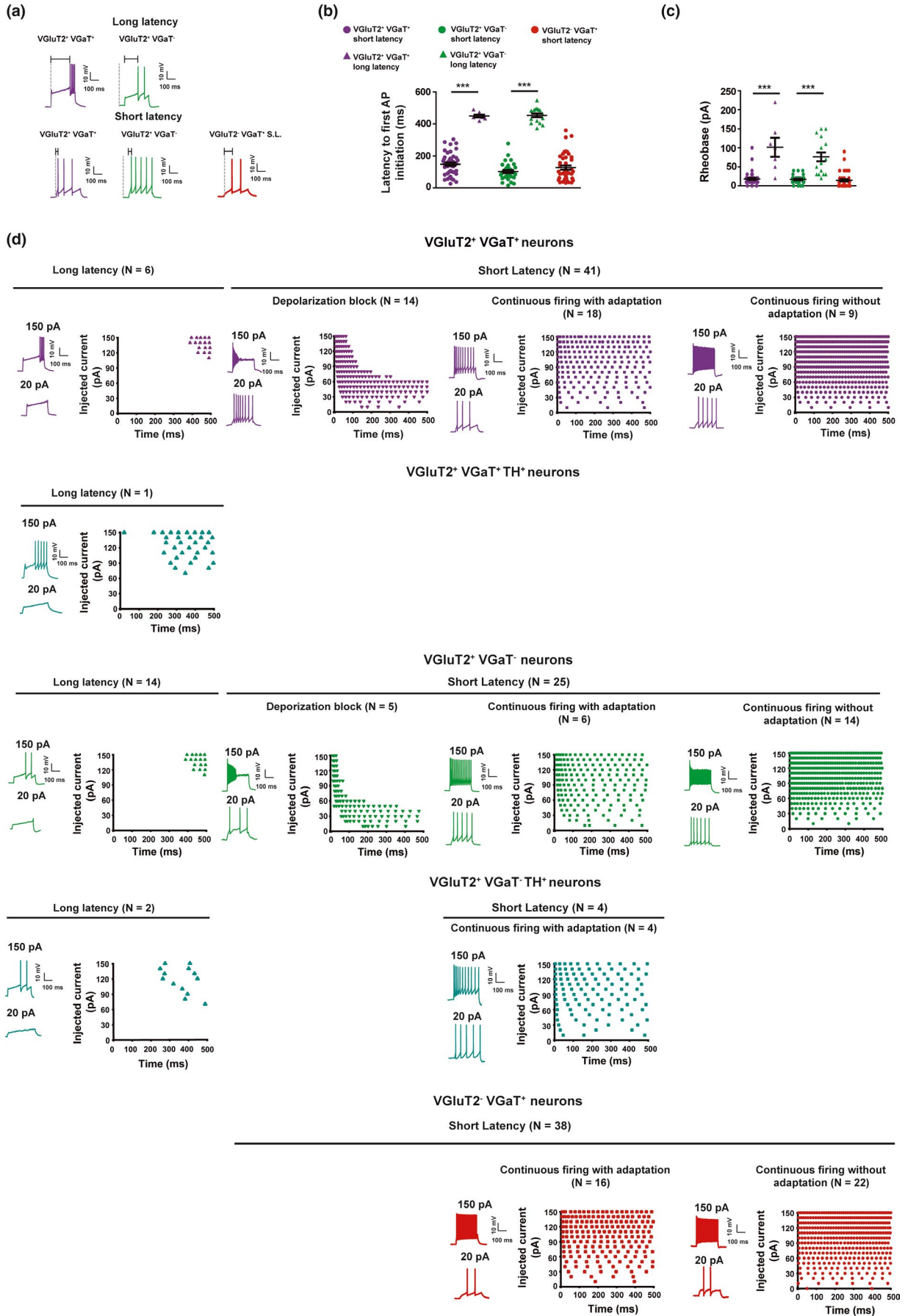


FIGURE 4 VGluT2⁺ VGaT⁺, VGluT2⁺ VGaT⁻, and VGluT2⁻ VGaT⁺ neurons co-expressing TH. (a) Co-localization of EYFP, biocytin, and TH in a recorded VTA neuron. Scale bar = 20 μm (b) Proportion of reconstructed VGluT2⁺ VGaT⁺, VGluT2⁺ VGaT⁻, and VGluT2⁻ VGaT⁺ neurons that lacked or expressed TH (TH⁺). (c) Example voltage clamp (top; step from -60 mV to -120 mV, 1 s duration) and current clamp (bottom; step from 0 pA to 50 to 100 pA to reach V_m = -120 mV) traces of I_h measurements in VTA VGluT2⁺ VGaT⁺ TH⁺ and VGluT2⁺ VGaT⁻ TH⁺ neurons

FIGURE 5 Stimulated firing patterns of VTA VGluT2⁺ VGaT⁺, VGluT2⁺ VGaT⁻, and VGluT2⁻ VGaT⁺ neurons. (a) Example current clamp traces of VTA neurons with long or short latency to firing in response to injected current steps. (b) VGluT2⁺ VGaT⁺, VGluT2⁺ VGaT⁻, and VGluT2⁻ VGaT⁺ neurons with short or long latency to first AP. One-way ANOVA $F_{4,139} = 107.8$ $p < 0.0001$, Tukey's *post hoc* test $***p < 0.0001$ (c) Evoked AP firing in VGluT2⁺ VGaT⁺, VGluT2⁺ VGaT⁻, and VGluT2⁻ VGaT⁺ neurons. Neurons with long latency to firing mostly required current injections > 40 pA to fire. One-way ANOVA $F_{4,13} = 32.49$ $p < 0.0001$, Tukey's *post hoc* test $***p < 0.0001$. (d) Example firing patterns in response to injected current steps sorted by long or short latency to firing. Short latency firing VGluT2⁺ VGaT⁺ and VGluT2⁺ VGaT⁻ neurons went into depolarization block, showed continuous firing with adaptation, or showed continuous firing without adaptation. VGluT2⁻ VGaT⁺ neurons only showed responses of continuous firing with or without adaptation. VGluT2⁺ VGaT⁺ TH⁺ neuron had long latency firing while VGluT2⁺ VGaT⁻ TH⁺ neurons had long latency firing or continuous firing with adaptation



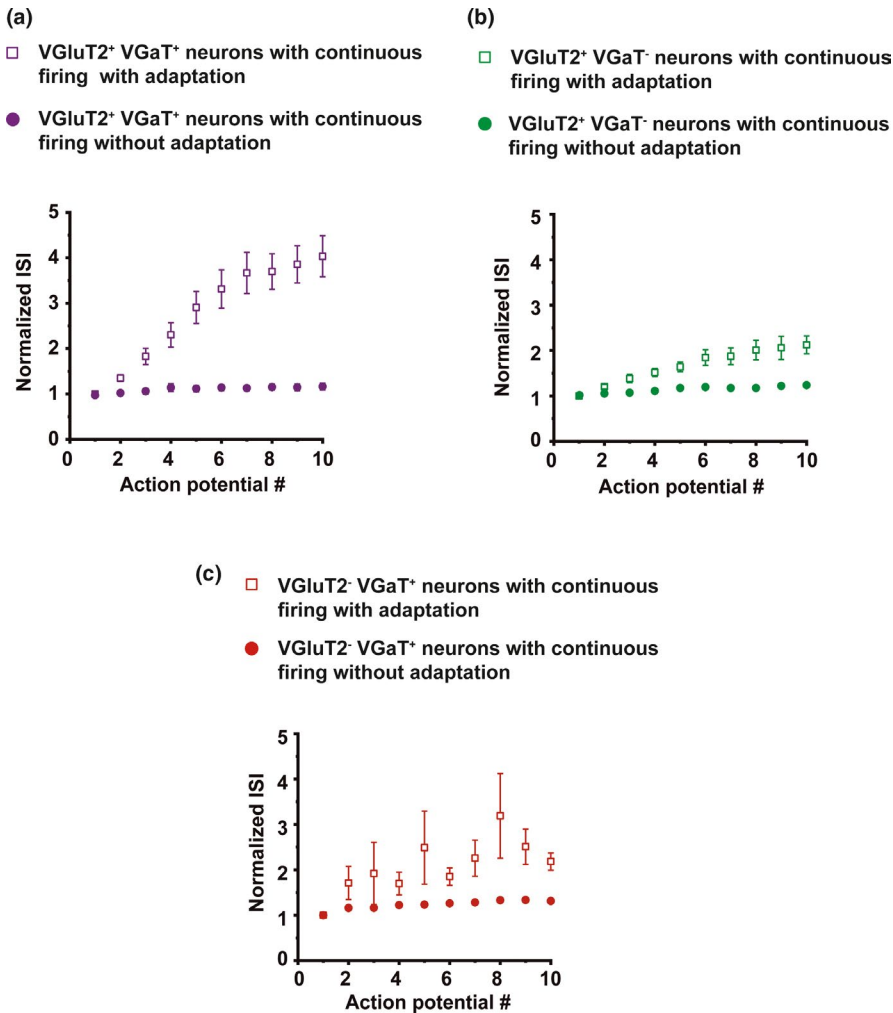
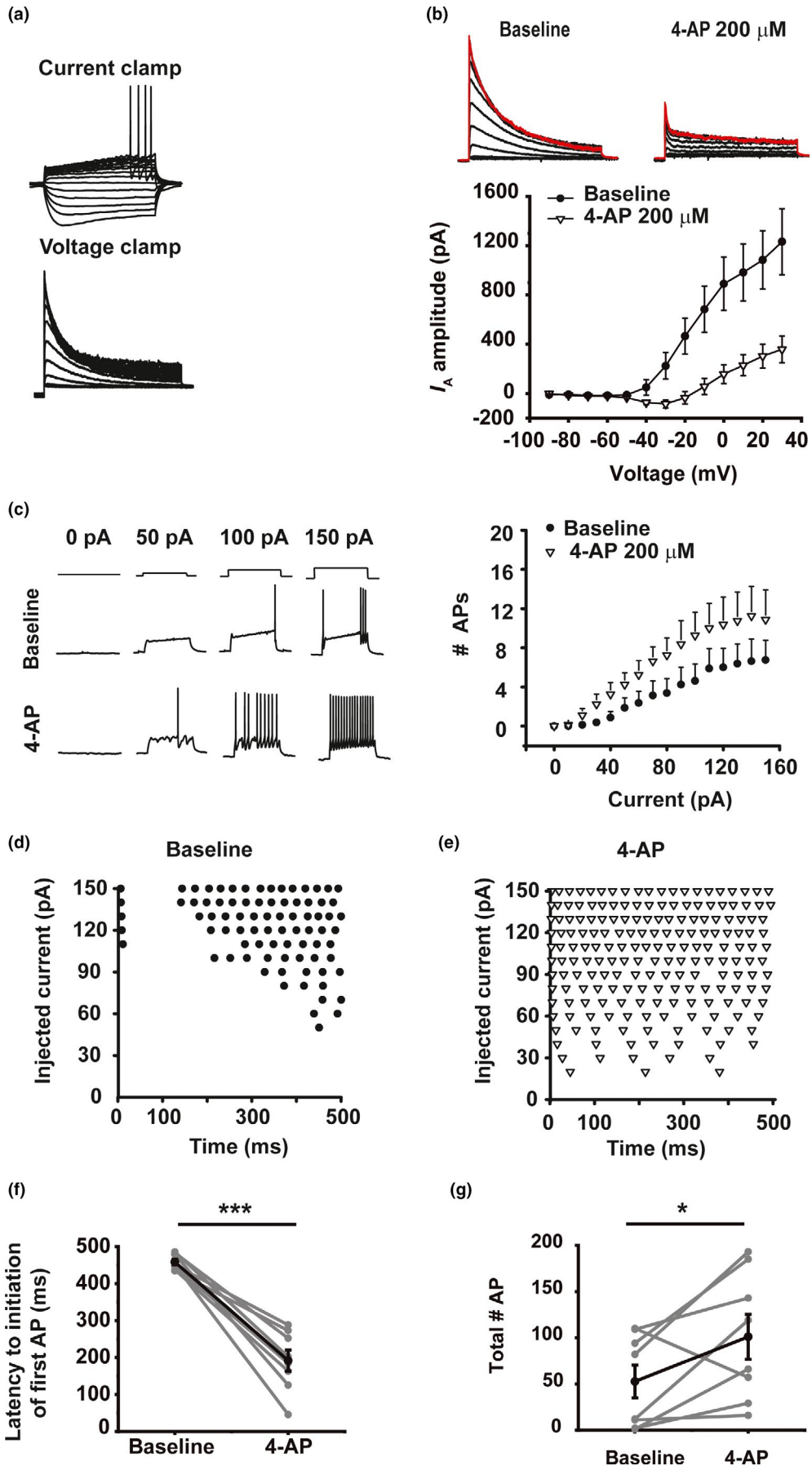


FIGURE 6 The change in interspike interval (ISI) across AP firing differentiate neurons with adaptation from neurons without adaptation. Normalized ISI of the first 10 AP fired after 150 pA current injection from VGluT2⁺ VGaT⁺ neurons with adaptation and without adaptation (a), VGluT2⁺ VGaT⁻ neurons with adaptation and without adaptation (b), and VGluT2⁻ VGaT⁺ neurons with adaptation and without adaptation (c)

(29/45 neurons, 22 mice; 122 ± 16 ms latency; Figure 5a-b,d; 4/29 neurons expressed TH; Figure 5d) and fewer long latency responses with a depolarizing ramp leading to firing (16/45 neurons, 13 mice; 454 ± 11 ms latency; Figure 5a-b,d; 2/16 neurons expressed TH; Figure 5d). Among the neurons with depolarizing ramp responses (VGluT2⁺ VGaT⁺ and VGluT2⁺ VGaT⁻ neurons), we detected A-type K⁺ currents (I_A), which were blocked by the I_A blocker 4-Aminopyridine (4-AP; 200 μ M) (Figure 7a-b). In addition, we found that 4-AP application increased the total number of APs fired during an input-output curve (10–150 pA, 500 ms) (4 VGluT2⁺

VGaT⁺ neurons and 4 VGluT2⁺ VGaT⁻ neurons, eight mice; baseline = 52.6 ± 17.8 , 4-AP = 101.0 ± 24.3 ; Figure 6c,g) with decreased firing latency (4 VGluT2⁺ VGaT⁺ neurons and 4 VGluT2⁺ VGaT⁻ neurons, 8 mice; baseline = 458 ± 7 ms, 4-AP = 192 ± 29 ms; Figure 6f). Compared to neurons expressing VGluT2 (VGaT⁺ or VGaT⁻), we found that all recorded VGluT2⁻ VGaT⁺ neurons had short latency firing responses to depolarizing current steps (38 neurons, 18 mice, 128 ± 13 ms latency; Figure 5a-b,d), and a subset showed frequency adaptation (22/38 neurons, 15 mice) (Figure 5d). Collectively, these results demonstrate that

FIGURE 7 I_A contributes to long latency firing in response to depolarization. (a) Example current clamp (top) and voltage clamp (bottom) traces in a VGluT2⁺ VGaT⁻ long latency neuron. (b) Example voltage clamp traces from a VGluT2⁺ VGaT⁻ long latency neuron at baseline and after bath application of the I_A blocker 4-Aminopyridine (4-AP) (top). Mean I_A amplitude responses across different voltage steps at baseline (close circles) and after bath application of 4-AP (open triangles) (bottom) ($n = 12$ neurons, 3 VGluT2⁺ VGaT⁺ neurons and 9 VGluT2⁺ VGaT⁻). (c) Example current clamp traces (left) of a long latency VGluT2⁺ VGaT⁺ neuron during depolarizing step current injections before and after bath application of 4-AP. Right, Input output summary graph shows 4-AP (open triangles) increased number of APs fired in response to depolarizing current injections compared to baseline (closed circles) ($n = 8$ neurons, 4 VGluT2⁺ VGaT⁺ neurons and 4 VGluT2⁺ VGaT⁻ neurons) Two way ANOVA 4-AP \times current $F_{15,112} = 0.83$, $p = 0.6408$, 4-AP $F_{15,112} = 49.06$, $p < 0.0001$, current $F_{15,112} = 4.64$, $p < 0.0001$. (d-e) Example firing pattern during injected current steps in a VGluT2⁺ VGaT⁺ long latency neuron at baseline (d) and after bath application of 4-AP (e). (f) 4-AP decreased the latency to AP firing during the rheobase step in long latency neurons ($n = 8$ neurons, 4 VGluT2⁺ VGaT⁺ and 4 VGluT2⁺ VGaT⁻). Paired t -test $t_7 = 8.877$, $***p < 0.0001$ (g) 4-AP increased total number of APs fired after activation across long latency neurons during an input output curve (10–150 pA, 500 ms). Paired t -test $t_7 = 2.426$, $*p = 0.0457$ ($n = 8$ neurons, 4 VGluT2⁺ VGaT⁺ and 4 VGluT2⁺ VGaT⁻)



both glutamate-GABA co-releasing (VGluT2⁺ VGaT⁺) and glutamate-releasing (VGluT2⁺ VGaT⁻) neurons are more heterogeneous in their firing properties than GABA-releasing (VGluT2⁻ VGaT⁺) neurons.

Given that previous studies have shown hyperpolarization-induced rebound burst firing in a subset of VTA dopamine and non-dopamine neurons mediated by I_h (Tateno & Robinson, 2011) or T-type calcium channels (Tracy et al., 2018; Woodward et al., 2019), we next tested the extent to which rebound firing occurs in these VTA neural subpopulations. After holding the membrane potential at -100 mV for 1 s and releasing that clamp, approximately 25% of VGluT2⁺ VGaT⁺ neurons showed rebound firing with short bursts of 2–4 APs (12/48 neurons, 10 mice; Figure 8a–b), and this response was stable over repeated trials (Figure 8e). In some of these neurons we tested whether the I_h blocker ZD 7,288 stopped rebound firing and found that it did in 2/4 neurons. In a different set of neurons, we found that the T-type calcium channel blocker mibefradil blocked rebound firing in 3/5 neurons. We also observed that 35% of VGluT2⁺ VGaT⁻ neurons (16/45 neurons, 11 mice) had rebound firing that was blocked by ZD 7,288 (7/7 tested neurons) or mibefradil (2/4 tested neurons) (Figure 8c–e). In contrast, we found that half (20/38 neurons, 14 mice) of the VGluT2⁻ VGaT⁺ neurons showed rebound firing, and this was blocked by ZD 7,288 (5/6 tested neurons) or mibefradil (2/5 tested neurons) (Figure 8). These findings demonstrate that subsets of each type of VTA neuron have rebound firing mediated by I_h and T-type calcium channels.

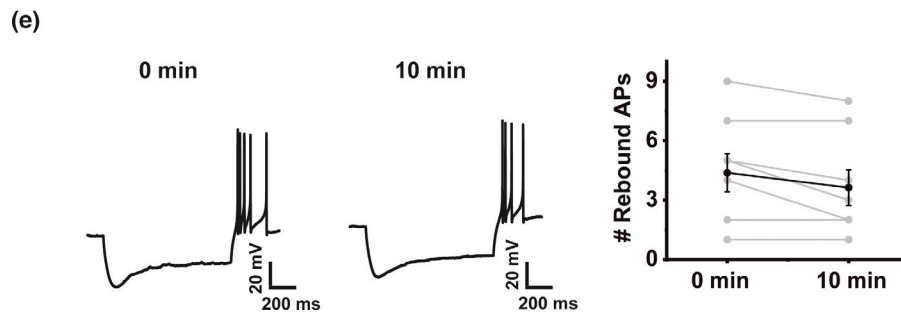
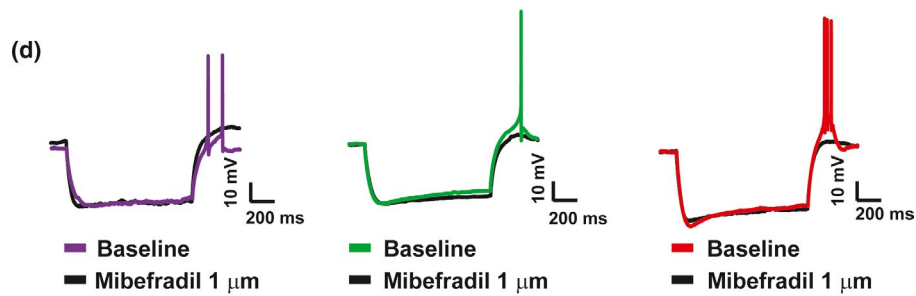
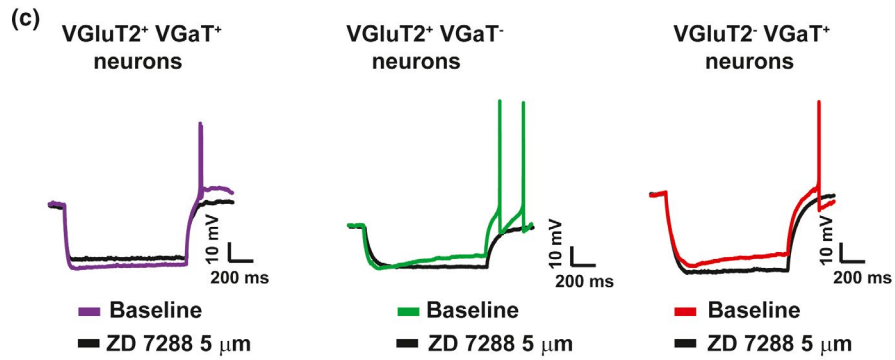
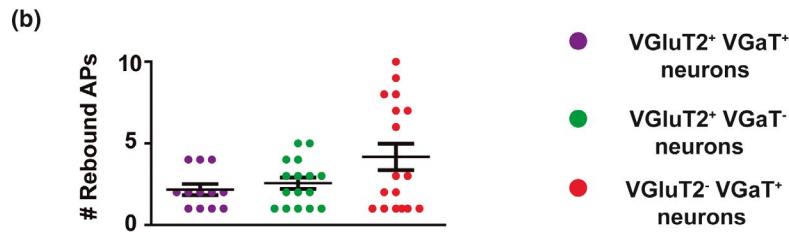
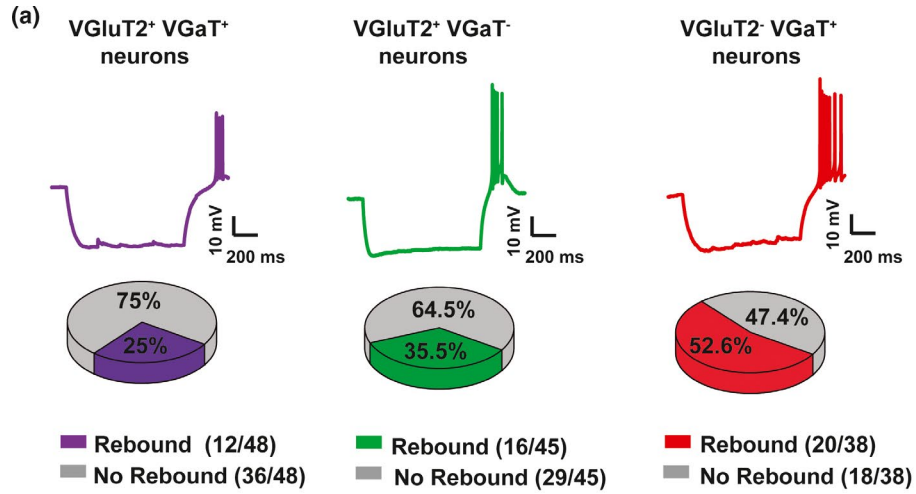
3.4 | VTA neuronal clustering by electrophysiological properties

We next evaluated the extent to which the electrophysiological properties described above grouped together by applying a cluster analysis based on K-means clustering and similarity parametric (Pearson's correlation coefficient) on the firing and intrinsic property data (Figure 9a). With this approach, we found four distinctive clusters of firing features, but these clusters did not correspond to our three neurotransmitter phenotypes (Figure 9b). For the 131 clustered neurons, 36.6% (48/131 neurons, 33 mice) grouped in cluster 1, 32.1%

(42/131 neurons, 31 mice) in cluster 2, 13.7% (18/131 neurons, 11 mice) in cluster 3, and 17.6% (23/131 neurons, 20 mice) in cluster 4 (Figure 9b).

In cluster 1 (48 neurons), 39.5% were VGluT2⁺ VGaT⁺ (19/48 neurons, 12 mice), 18.8% were VGluT2⁺ VGaT⁻ (9/48 neurons, seven mice), and 41.6% were VGluT2⁻ VGaT⁺ (20/48 neurons, 15 mice) (Figure 9b). Neurons grouped within cluster 1 were characterized by a sustained AP firing with marked adaptation (46.5 ± 2.8 Hz maximal AP frequency, Figure 8h), and depolarized membrane potential (-61.9 ± 0.8 mV; Figure 8e). We found that 75% of the neurons within this cluster were spontaneously active during cell attached recordings (36/48 neurons, 29 mice), representing the highest percentage of spontaneously active neurons among the four different clusters. In cluster 2, 21.4% were VGluT2⁺ VGaT⁺ (9/42 neurons, 8 mice), 35.7% were VGluT2⁺ VGaT⁻ (15/42 neurons, 12 mice), and 42.8% were VGluT2⁻ VGaT⁺ neurons (18/42 neurons, 12 mice) (Figure 9b). The neurons in this cluster had small rheobase (11.6 ± 1.4 pA; Figure 9f), short latency AP firing in response to depolarizing current (97 ± 10 ms Figure 8g), and sustained firing with minimal frequency adaptation in response to current steps (76.1 ± 3.4 Hz; Figure 8h). We found that 69% (29/42 neurons, 23 mice) of the neurons in this cluster showed rebound firing after release from clamp induced hyperpolarization. In cluster 3, 72.2% were VGluT2⁺ VGaT⁺ (13/18 neurons, 8 mice) and 27.8% were VGluT2⁺ VGaT⁻ neurons (5/18 neurons, 4 mice; Figure 9b). Neurons grouped in this cluster exhibited rapid depolarization block during low magnitude depolarizing current steps (Figure 9c,d). In cluster 4, 30.4% (5/23 neurons from 5 mice) were VGluT2⁺ VGaT⁺ and 69.5% were VGluT2⁺ VGaT⁻ neurons (16/23 neurons, 14 mice). No VGluT2⁻ VGaT⁺ neurons were classified to this cluster. Neurons in cluster 4 had larger rheobase (83.9 ± 11.1 pA; Figure 9f), long latencies to AP firing in response to injected current (452 ± 11 ms; Figure 9g), a depolarizing ramp before the onset of AP firing in response to current steps (Figure 9c–e), and included some neurons with I_A (Figure 8c–g). We found that all neurons within cluster 4 were quiescent during cell attached recordings. To evaluate whether differences in membrane potential among the clusters of neurons influence their intrinsic properties, we analyzed the relationship between the membrane potential and rheobase, latency,

FIGURE 8 Rebound firing is mediated by I_h and T-type calcium channels in VGluT2⁺ VGaT⁺, VGluT2⁺ VGaT⁻, and VGluT2⁻ VGaT⁺ neurons. (a) Example current clamp traces (top) and proportion of neurons showing rebound firing (bottom) among VGluT2⁺ VGaT⁺ (purple), VGluT2⁺ VGaT⁻ (green), and VGluT2⁻ VGaT⁺ (red) neurons. (b) Number of rebound APs fired by VGluT2⁺ VGaT⁺ (purple), VGluT2⁺ VGaT⁻ (green), and VGluT2⁻ VGaT⁺ (red) neurons. (c) Example recordings in which rebound firing was blocked by ZD 7,288 (5 μ M) (black traces). (d) Example recordings in which rebound firing was blocked by mibefradil (1 μ M) (black traces). (e) Left, example current clamp traces from a VGluT2⁻ VGaT⁺ neuron with rebound firing initially after initiating whole cell recording (0 min) and 10 min later. Right, summary number of rebound APs early (0 min) and late (after 10 min) ($n = 8$ neurons, 2 VGluT2⁺ VGaT⁺ neurons, 2 VGluT2⁺ VGaT⁻ neurons, and 4 VGluT2⁻ VGaT⁺ neurons)



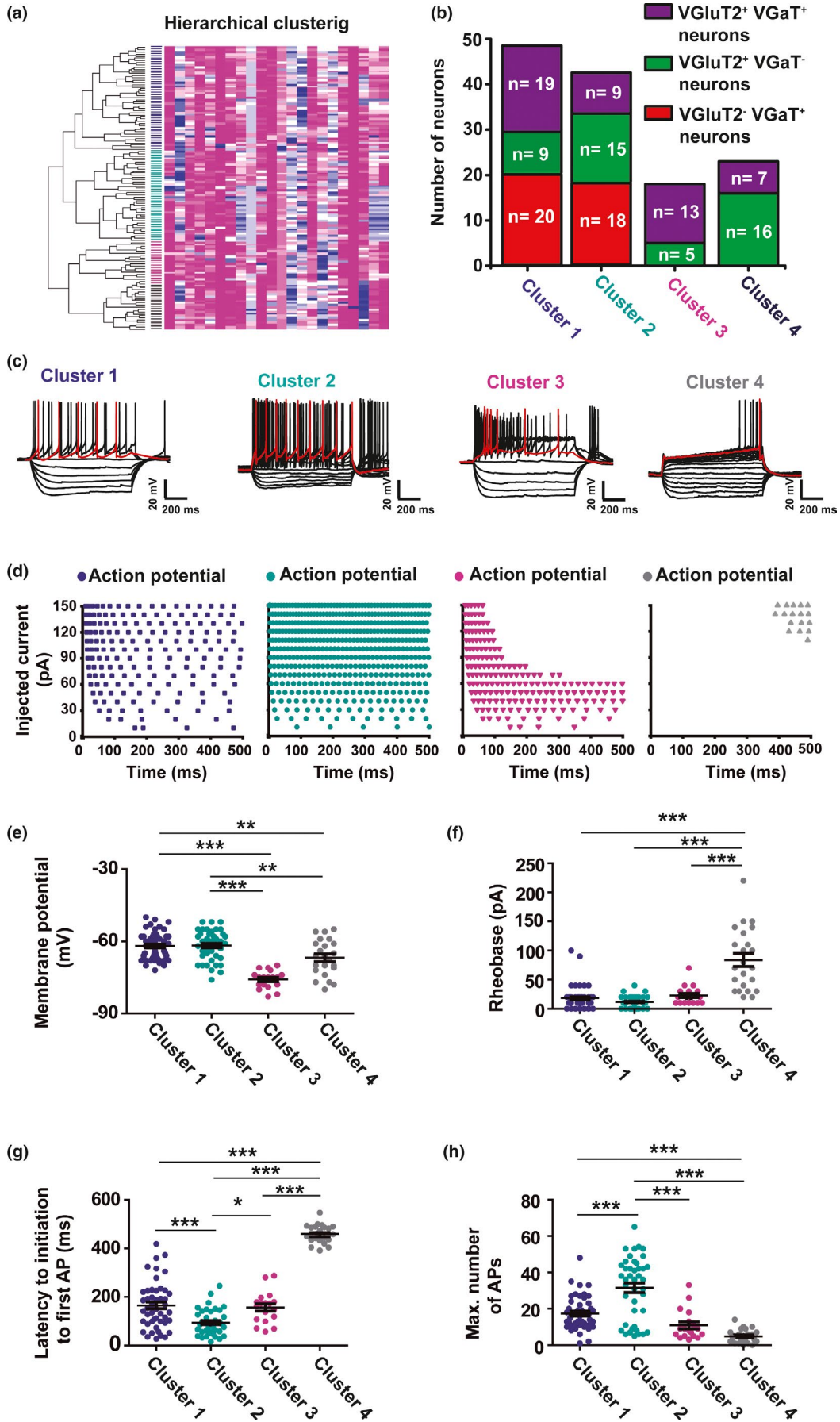


FIGURE 9 Hierarchical cluster analysis of electrophysiological properties of VTA VGluT2⁺ VGaT⁺, VGluT2⁺ VGaT⁻, and VGluT2⁻ VGaT⁺ neurons. (a) Dendrogram and heat map of VTA neuronal electrophysiological properties. (b) Neurotransmitter neuronal phenotype distributions across clusters. (c) Example current clamp traces from neurons within each cluster in response to hyperpolarizing and depolarizing current injections. (d) Examples of firing patterns over time during depolarization steps in neurons within each cluster. (e) Membrane potentials of neurons in each cluster. One-way ANOVA $F_{3,130} = 28.25$, $p < 0.0001$, Tukey's *post hoc* test $**p < 0.001$ $***p < 0.0001$. (f) Rheobase of neurons in each cluster. One-way ANOVA $F_{3,130} = 42.45$, $p < 0.0001$, Tukey's *post hoc* test $***p < 0.0001$. (g) Latency to fire APs in response to depolarizing current steps in neurons in each cluster. One-way ANOVA $F_{3,130} = 134.9$, $p < 0.0001$, Tukey's *post hoc* test $*p < 0.05$ $***p < 0.0001$. (h) Maximum number of APs fired during depolarizing current steps (500 ms) of neurons in each cluster. One-way ANOVA $F_{3,130} = 30.64$, $p < 0.0001$, Tukey's *post hoc* test $*p < 0.05$ $***p < 0.0001$

and maximum number of APs fired. We found that the membrane potential did not correlate with rheobase ($r^2 = 0.08$) (Figure 10a-b), latency ($r^2 = 0.04$) (Figure 10c-d), or the maximum number of APs fired ($r^2 = 0.03$) (Figure 10e-f). Therefore resting membrane potential differences are not the main physiological cause of the property differences between clusters.

Next, we determined whether the four identified clusters had specific topographical distribution within the VTA by mapping the locations of the recorded neurons. We found cluster 1 neurons in ventral and middle VTA, with a dorsal to ventral, and lateral to medial increasing gradient of distribution (Figure 11b). We frequently observed cluster 2 neurons in middle VTA concentrated more medially (Figure 11c), cluster 3 neurons in the ventral and middle VTA also enriched medially (Figure 11d), and cluster 4 neurons in the middle and dorsal VTA confined to the most medial part of the VTA (Figure 11e). These findings indicate that VGluT2⁺ VGaT⁺, VGluT2⁺ VGaT⁻, and VGluT2⁻ VGaT⁺ neurons have a topographic organization more related to shared electrophysiological properties rather than to the neurotransmitter that they release.

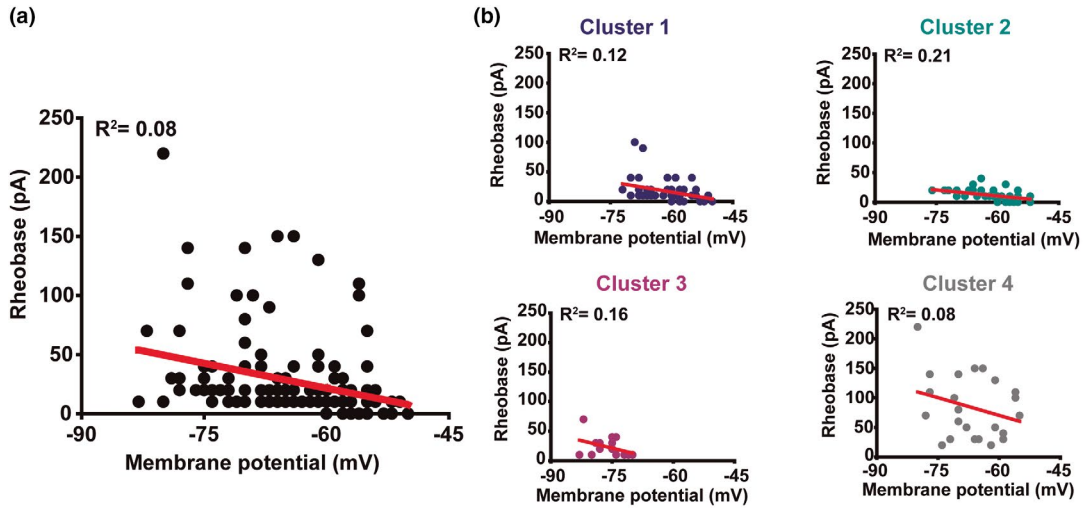
3.5 | μ -opioid receptors (MORs) are present in VTA GABA-releasing and glutamate-releasing neurons

Given that previous electrophysiological studies have demonstrated the presence of MORs in a subset of VTA GABA releasing neurons (Margolis et al., 2012), and anatomical studies have documented expression of Oprm1 mRNA (gene encoding MOR) in VTA VGluT2 neurons (Kudo et al., 2014), we systematically analyzed Oprm1 mRNA expression in VTA neurons that express VGluT2 mRNA or VGaT mRNA. We detected Oprm1 mRNA in VGluT2⁺ VGaT⁻ (Figure 12a), VGluT2⁻ VGaT⁺ (Figure 12b), and VGluT2⁺ VGaT⁺ neurons in coronal mouse sections (Figure 12c). We determined that within the total population of VTA VGluT2⁺ VGaT⁺ neurons, 43 of 1,268 neurons co-expressed Oprm1 mRNA. These VGluT2⁺ VGaT⁺ neurons co-expressing Oprm1 mRNA represented $2.5 \pm 0.2\%$ of the total population of VTA neurons expressing Oprm1 mRNA (43 / 1,718 neurons,

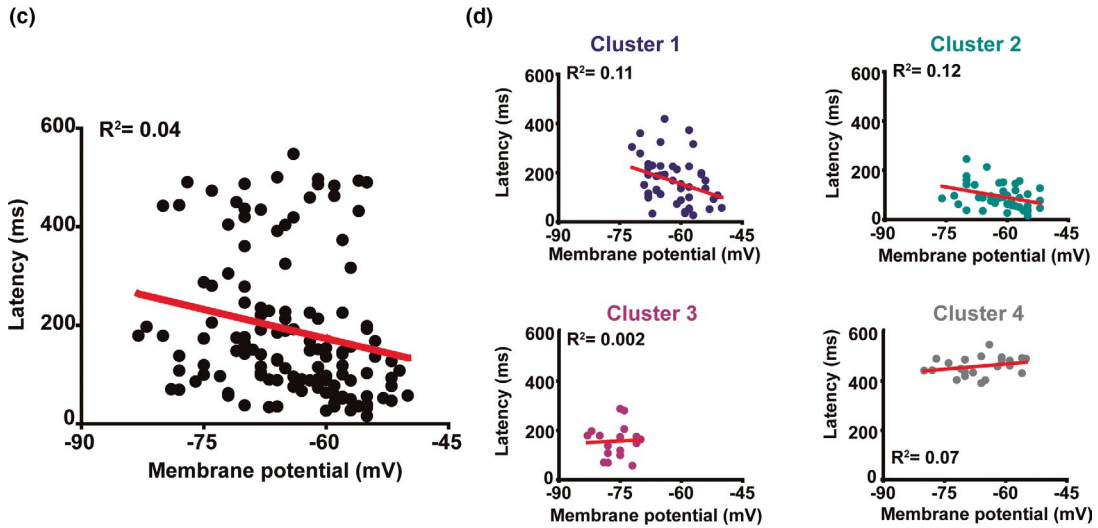
three mice; Figure 12d). We found that within the total population of VGluT2⁺ VGaT⁻ neurons, 336 of 8,028 neurons co-expressed Oprm1 mRNA. These VGluT2⁺ VGaT⁻ neurons co-expressing Oprm1 mRNA represented $19.6 \pm 1.9\%$ of the total population of VTA neurons expressing Oprm1 (336 / 1,718 neurons, three mice; Figure 12d). We calculated that within the total population of VGluT2⁻ VGaT⁺ neurons, 1,337 of 6,693 co-expressed Oprm1 mRNA. These VGluT2⁻ VGaT⁺ neurons co-expressing Oprm1 mRNA represented $77.8\% \pm 0.9\%$ of the total population of VTA neurons expressing Oprm1 (1,337 / 1,718 neurons, three mice; Figure 12d). These findings showed that GABA-releasing and glutamate-releasing neurons are two major classes of VTA neurons with the capability to synthesize MORs.

Next, we tested for responses to the MOR selective agonist DAMGO (1 μ M) in VGluT2⁺ VGaT⁺, VGluT2⁺ VGaT⁻, and VGluT2⁻ VGaT⁺ neurons. We did not detect an effect of DAMGO on the membrane potential of most VGluT2⁺ VGaT⁺ recorded neurons (change with DAMGO -0.7 ± 0.4 mV; -69.5 ± 2.0 mV baseline, -70.2 ± 2.2 mV DAMGO; 8 tested neurons) (Figure 12f-g), but only in one VGluT2⁺ VGaT⁺ recorded neuron DAMGO induced membrane potential hyperpolarization (change with DAMGO -4.4 mV; -75.4 mV baseline, -79.8 mV DAMGO) (Figure 12f). We detected DAMGO induced hyperpolarizations in a subset of VGluT2⁺ VGaT⁻ neurons (change with DAMGO -7.1 ± 1.7 mV; -64.3 ± 2.7 mV baseline, -71.4 ± 3.2 mV DAMGO, $n = 7$ of 17 tested neurons, 14 mice) (Figure 12f-g). Hyperpolarizations were also observed in the presence of the GABA_A receptor antagonist (bicuculline, 10 μ M) (Figure 12h). Application of the MOR selective antagonist CTAP (1 μ M) reversed the DAMGO-induced hyperpolarizations (-73.3 ± 3.1 mV baseline, -84.5 ± 2.7 mV DAMGO, -72.5 ± 3.4 mV DAMGO + CTAP, 5 tested neurons) (Figure 12j-k). Similarly, we detected DAMGO induced hyperpolarizations in just over half of VGluT2⁻ VGaT⁺ tested neurons (change with DAMGO -7.7 ± 1.3 mV; -64.1 ± 1.9 mV baseline, -71.8 ± 2.1 mV DAMGO, $n = 10$ out of 18 tested neurons, 15 mice) (Figure 12f-g), and these were also reversed by CTAP (-58.9 ± 1.0 mV baseline, -64.9 ± 1.2 mV DAMGO, -60.5 ± 1.2 mV DAMGO + CTAP, 6 tested neurons) (Figure 12j-k). Collectively, these findings indicate that a subset of VTA neurons that release either GABA or

Membrane potential vs rheobase



Membrane potential vs latency



Membrane potential vs maximum number of APs

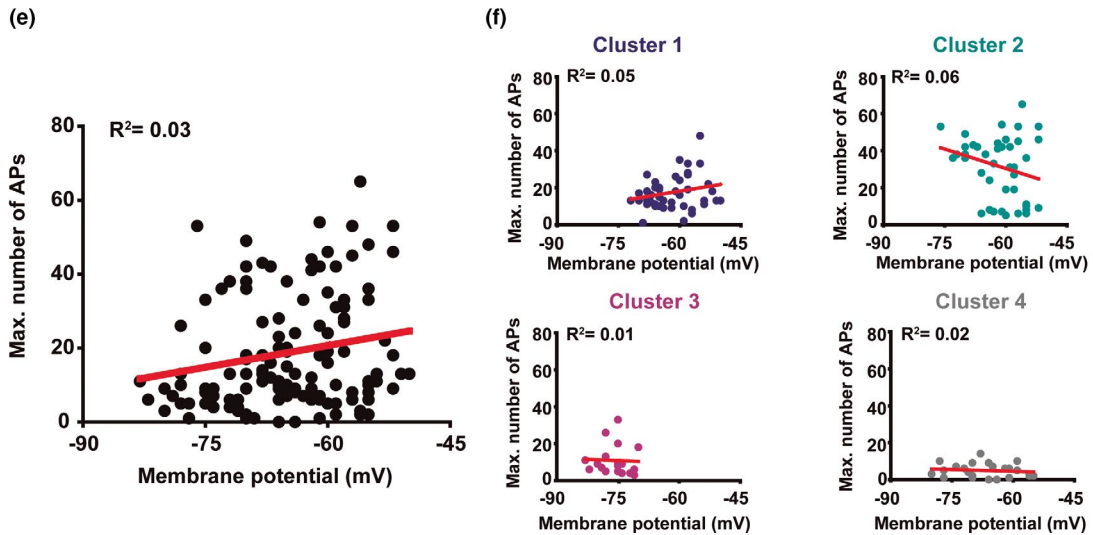


FIGURE 10 Resting membrane potential does not underly the differences in firing properties of VTA neurons. (a-b) Correlation analysis of membrane potential and rheobase of recorded neurons overall (a) and separated into clusters (B). (c-d) Correlation analysis of membrane potential and latency to fire APs in response to depolarizing current steps across all recorded neurons (c) and separated into clusters (d). (e-f) Correlation analysis of membrane potential and the maximum number of APs fired during depolarizing current steps (500 ms) of all recorded neurons (e) and neurons separated into clusters (f)

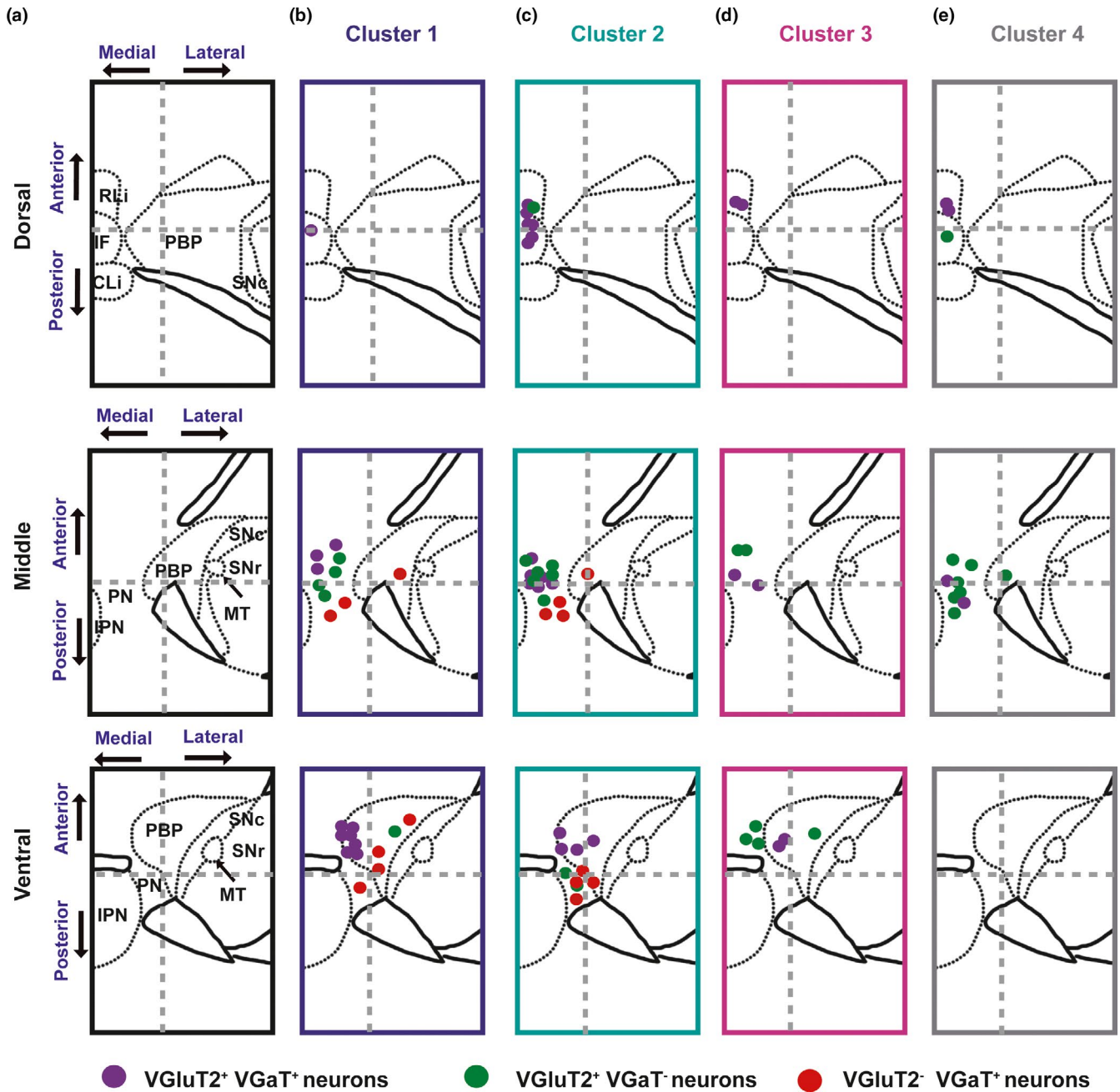


FIGURE 11 Topographic locations of VTA neurons by physiological cluster. (a) Schematic representations of dorsal, middle, and ventral horizontal VTA slices. (b-e) Locations of recorded neurons from cluster 1 (b), cluster 2 (c), cluster 3 (d), and cluster 4 (e) in dorsal, middle, and ventral horizontal VTA slices. Vertical grey dashed line divides the medial and lateral VTA. Each circle represents a single recorded neuron

glutamate express functional MOR in their somatodendritic region, the activation of which results in hyperpolarization.

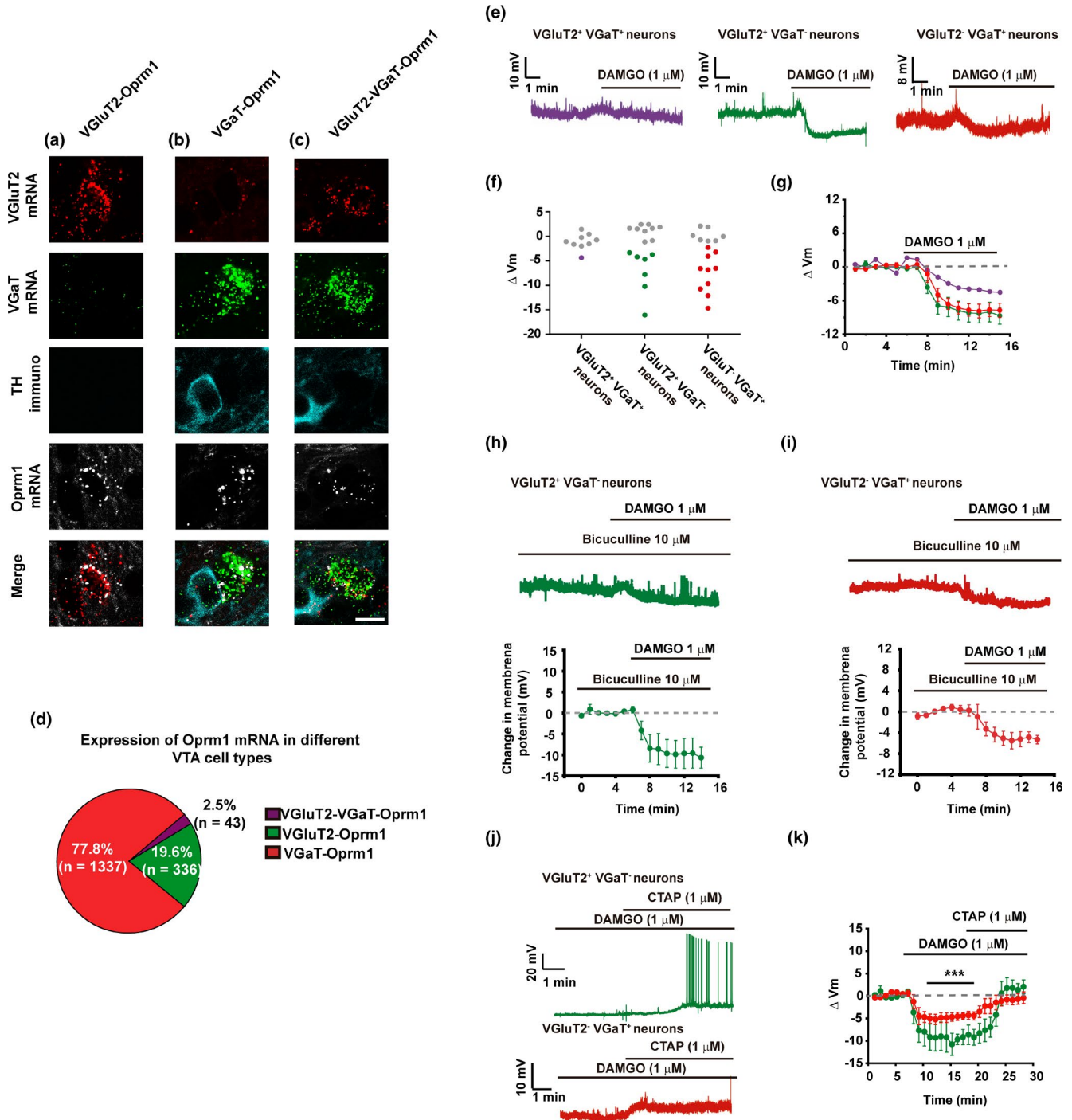
4 | DISCUSSION

The VTA has historically been conceptualized as brain structure dominated by dopaminergic neurons, and the properties of these neurons have been intensively investigated for decades. However, the VTA has three additional major classes of neurons: GABA-releasing (VGluT2⁻ VGaT⁺), glutamate-releasing (VGluT2⁺ VGaT⁻), and glutamate-GABA co-releasing (VGluT2⁺ VGaT⁺) neurons, whose physiological properties were previously unknown. To specifically study these three classes of neurons, we selectively tagged each class using in vivo expression of eYFP after intra-VTA delivery of INTRSECT viral vectors (C_{ON}/F_{ON}, C_{ON}/F_{OFF} or C_{OFF}/F_{ON}) in different cohorts of double transgenic *vglut2-Cre/vgat-Flp* mice. We validated the selective expression of eYFP in each of the three targeted classes of VTA neurons by demonstrating that: (1) most of the VTA transduced neurons with C_{ON}/F_{ON} viral vector (for targeting glutamate-GABA co-releasing neurons) co-expressed VGluT2 and VGaT mRNAs, (2) those transduced with C_{ON}/F_{OFF} viral vector (for targeting glutamate-releasing neurons) expressed VGluT2 mRNA without VGaT mRNA, and (3) those transduced with C_{OFF}/F_{ON} viral vector (for targeting GABA-releasing neurons) expressed VGaT mRNA without VGluT2 mRNA. Using ex vivo VTA recordings of the three classes of transduced neurons, we found that both glutamate-releasing and glutamate-GABA co-releasing neurons have lower excitability and lower basal firing activity than GABA-releasing neurons. In addition, while we observed diversity in the depolarization-induced firing patterns of glutamate-releasing and glutamate-GABA co-releasing neurons, the responses among GABA-releasing neurons were more uniform. We

also demonstrated that whereas the majority of the VTA neurons containing the μ opioid receptors (MORs) are GABA-releasing neurons and were hyperpolarized by MOR, some glutamate-releasing neurons also expressed MORs and were hyperpolarized by MOR activation. Collectively, we provide evidence that: (1) both VTA glutamate-releasing and glutamate-GABA co-releasing neurons require a stronger excitatory drive to fire than GABA-releasing neurons, and (2) postsynaptic MOR activation inhibits the activity of both GABA-releasing and glutamate-releasing VTA neurons.

It is well-documented that I_h is present in both dopamine and non-dopamine neurons (Jones & Kauer, 1999; Margolis et al., 2006), including neurons expressing GAD (Chiang et al., 2011; Margolis et al., 2012; Ntamati et al., 2018), VGaT (Woodward et al., 2019) or VGluT2 (Hnasko et al., 2012). We extended these observations by showing that I_h is present in less than half of the glutamate-GABA co-releasing neurons, about half of the glutamate-releasing neurons, and in close to 90% of the GABA-releasing neurons. The mean I_h magnitude is smallest in glutamate-GABA co-releasing neurons, followed by GABA-releasing neurons, and largest in glutamate-releasing neurons. We further determined that the I_h magnitude in both glutamate-GABA co-releasing and glutamate-releasing neurons was not related to the presence of TH. We found that regardless of the neuronal cell type, the neurons with the greatest I_h magnitudes were located in the lateral VTA, and those with low amplitudes were in the medial VTA. These findings are consistent with the VTA latero-medial neuronal heterogeneity observed in dopamine neurons (Li X et al. 2013; Morales & Margolis, 2017) and show that it is a property shared by all classes of VTA neurons. While the molecular bases underlying differences in I_h magnitude among VTA neurons remains to be determined, one possibility is varying levels of expression of the four hyperpolarization-activated cyclic nucleotide-gated channel (HCN1-4) subunits that generate I_h , whose transcripts have

FIGURE 12 Functional MORs are present in VTA VGluT2⁺ VGaT⁻ and VGluT2⁻ VGaT⁺ neurons. Detection of mRNA encoding VGluT2 (red), VGaT (green), or Oprm1 (white), and protein for TH (cyan). (a) An example neuron co-expressing VGluT2 and Oprm1 mRNAs. (b) An example neuron co-expressing VGaT and Oprm1 mRNAs. (c) An example neuron co-expressing VGluT2, VGaT, and Oprm1 mRNAs. (d) Proportion of VTA neurons expressing VGluT2 or VGaT mRNA with Oprm1 mRNA (3 mice). (e) Example current clamp traces from a VGluT2⁺ VGaT⁺ (left), VGluT2⁺ VGaT⁻ (middle), and a VGluT2⁻ VGaT⁺ (right) neuron during bath application of DAMGO. (f) DAMGO-induced changes in membrane potential in responsive and non-responsive VGluT2⁺ VGaT⁺, VGluT2⁺ VGaT⁻, and VGluT2⁻ VGaT⁺ neurons. Responsive neurons are displayed in purple, green, or red circles, and non-responsive neurons are represented by gray circles (g) Time course averages showing the time locked change in membrane potentials of responsive VGluT2⁺ VGaT⁺, VGluT2⁺ VGaT⁻, and VGluT2⁻ VGaT⁺ neurons during bath application of DAMGO. (h) Example current clamp trace of a VGluT2⁺ VGaT⁻ neuron that hyperpolarized in response to DAMGO in the presence of the GABA_A receptor antagonist bicuculline (top) and summary time course across VGluT2⁺ VGaT⁻ neurons ($n = 4$) to application of DAMGO in the presence of bicuculline (bottom). (i) Example current clamp trace of a DAMGO induced hyperpolarization of a VGluT2⁻ VGaT⁺ neuron in the presence of bicuculline (top) and summary time course across VGluT2⁻ VGaT⁺ neurons in response to DAMGO in the presence of bicuculline ($n = 5$) (bottom). (j) Example current clamp traces showing depolarizations in response to the μ -opioid receptor selective antagonist CTAP in neurons that were hyperpolarized by DAMGO. (k) Summary time courses to application of DAMGO and CTAP. Repeated measures ANOVA $F_{2,14} = 15.0$, $p < 0.0003$, Dunnett's multiple comparison test $p < 0.001$ for VGluT2⁺ VGaT⁻; $F_{2,17} = 3.638$, $p < 0.0011$, Dunnett's multiple comparison test $p < 0.001$ for VGluT2⁻ VGaT⁺



been detected in the VTA (Monteggia et al., 2000). As an alternative, differences in I_h magnitude may reflect differential neuronal distribution of the HCN channels across neuronal compartments, as the HCN subunits have been detected in the plasma membrane of cell bodies, dendrites, or axons (Notomi & Shigemoto, 2004).

While our findings on the intrinsic properties of VTA neurons suggest that stronger excitatory drive is required for firing in VTA glutamate-releasing and glutamate-GABA co-releasing neurons compared to VTA GABA-releasing neurons, it remains to be determined which excitatory sources

target each class of VTA neuron. Ultrastructural and electrophysiological reports indicate that VTA neurons expressing either GAD or VGaT receive excitatory input from different brain areas. For instance, pioneer ultrastructural studies showed that VTA GABA-neurons (expressing GAD) receive asymmetric (excitatory-type) synapses from axon terminals whose neurons originate in the lateral habenula (Olmelchenko et al., 2009), medial prefrontal cortex (Carr & Sesack, 2000), periaqueductal grey (Olmelchenko & Sesack, 2010), and bed nucleus of the stria terminalis (Kudo et al., 2012). Furthermore, recent findings utilizing optogenetics and VTA

slice electrophysiology have shown that the firing of GABA neurons (expressing VGaT or GAD) is evoked by exciting glutamatergic inputs (expressing VGlut2) from lateral hypothalamus neurons (Nieh et al., 2015), superior colliculus neurons (Zhou et al., 2019) or periaqueductal grey neurons (Ntamati et al., 2018). Moreover, a circuitry-based study on input from the periaqueductal grey to VTA showed that periaqueductal grey glutamatergic neurons preferentially target the GAD neurons with large I_h (Ntamati et al., 2018). It is possible that some of the GABA neurons identified in these prior studies were in fact glutamate-GABA co-releasing neurons. While information on glutamatergic afferents to VTA glutamatergic neurons is limited, we recently reported quantitative ultrastructural, optogenetic, and electrophysiological evidence showing that VTA glutamate-releasing neurons ($VGlut2^+ VGaT^-$) receive a strong glutamatergic input from the lateral hypothalamic area, LHA (Barbano et al., 2020). Furthermore, we also showed that the somatodendritic region of a single VTA glutamate-releasing neuron receives multiple asymmetric synapses from axon terminals arising from LHA glutamatergic neurons (Barbano et al., 2020). Combining basal physiological neural properties with how these and other yet to be characterized inputs will be activated at varying strengths across behavioral contexts yields the neural computation(s) that the different VTA neural subtypes perform.

Previous studies found hyperpolarization-induced rebound burst firing in subsets of VTA dopamine and non-dopamine neurons mediated by I_h (Tateno & Robinson, 2011) or T-type calcium channels (Tracy et al., 2018; Woodward et al., 2019). We found the same types of responses in subpopulations of glutamate-GABA co-releasing, glutamate-releasing, and GABA-releasing neurons. A recent VTA electrophysiological study in a knock-in rat line expressing the fluorescent protein Venus in VGaT neurons, reported two populations of VTA GABA neurons expressing T-channels with different rebound firing properties (type 1 with low threshold calcium spikes during rebound firing, and type two with post hyperpolarizing action potentials during rebound firing) (Woodward et al., 2019). Given that we detected T-channel mediated rebound in glutamate-GABA co-releasing and GABA-releasing neurons, and both classes of neurons express VGaT (Root et al., 2018), one possibility is that our results correlate with the two response types detected in rat VTA VGaT-Venus neurons.

Findings from electrophysiological and pharmacological studies show presynaptic and postsynaptic MOR function in the VTA (Johnson & North, 1992; Margolis et al., 2012; Fields and Margolis, 2015). While postsynaptic MORs are classically thought to be limited to GABA neurons within the VTA, we observed transcripts encoding MORs (Oprm1) expressed in a subset of glutamate-releasing neurons, and these neurons were clustered in the midline aspects of the VTA.

We also found that MOR activation hyperpolarizes these glutamate-releasing neurons. These observations together with the presence of MORs in synaptic terminals impinging on VTA neurons (Bull et al., 2017; Chen et al., 2015; Margolis et al., 2005; Zhang et al., 2015) underscore the complex actions of opioids within the VTA.

In summary, we detected unique as well as overlapping electrophysiological properties among the VTA glutamate-GABA co-releasing, glutamate-releasing, and GABA-releasing neurons. Our electrophysiological findings indicate that firing of VTA glutamate-GABA co-releasing and glutamate-releasing neurons may require stronger excitatory drive compared to the GABA-releasing neurons. However, given that the neuronal firing pattern depends on both the intrinsic properties of the neurons and the network activity innervating them, future studies are necessary to identify the origin, nature, and impact of inputs to the specific classes of VTA neurons.

5 | DECLARATION OF INTERESTS

The authors declare no competing interests.

ACKNOWLEDGMENTS

This work was supported by the Intramural Research Program of the National Institute on Drug Abuse and R01DA042025 grant (EBM). We also thank Dr. Nirmath Sah (JHU) for advice on cluster analysis. We also thank the NIDA/IRP Confocal and Electron Microscopy Core for collecting confocal images.

AUTHOR CONTRIBUTIONS

MM and JM-B conceptualized and initiated the project. JM-B and IC performed electrophysiological studies. JM-B, IC, GEM-S, and EBM analyzed electrophysiological data. SM, HW, and BL performed immunolabeling studies and quantified neurons from RNAscope studies. H-LW and BL performed RNAscope studies. SZ performed confocal studies and data analysis. MM, JM-B, and EBM prepared the manuscript with contributions from all authors.

PEER REVIEW

The peer review history for this article is available at <https://publons.com/publon/10.1111/ejn.15156>.

DATA AVAILABILITY STATEMENT

Supporting data are available.

ORCID

Jorge Miranda-Barrientos  <https://orcid.org/0000-0003-1161-5695>

REFERENCES

- Barbano, M. F., Wang, H.-L., Zhang, S., Miranda-Barrientos, J., Estrin, D. J., Figueroa-Gonzalez, A., Liu, B., Barker, D. J., & Morales, M. (2020). VTA glutamatergic neurons mediate innate defensive behaviors. *Neuron*.
- Berridge, K. C. (2007). The debate over dopamine's role in reward: The case for incentive salience. *Psychopharmacology (Berl)*, *191*(3), 391–431.
- Bromberg-Martin, E. S., Matsumoto, M., & Hikosaka, O. (2010). Dopamine in motivational control: Rewarding, aversive, and alerting. *Neuron*, *68*(5), 815–834. <https://doi.org/10.1016/j.neuron.2010.11.022>. Review
- Bull, F. A., Baptista-Hon, D. T., Lambert, J. J., Walwyn, W., & Hales, T. J. (2017). Morphine activation of mu opioid receptors causes disinhibition of neurons in the ventral tegmental area mediated by β -arrestin2 and c-Src. *Scientific Reports*, *7*, 9969. Published online 2017 Aug 30. <https://doi.org/10.1038/s41598-017-10360-8>
- Carr, D. B., & Sesack, S. R. (2000). GABA-containing neurons in the rat ventral tegmental area project to the prefrontal cortex. *Synapse (New York, N. Y.)*, *38*(2), 114–123.
- Chen, M., Zhao, Y., Yang, H., Luan, W., Song, J., Cui, D., Dong, Y., Lai, B., Ma, L., & Zheng, P. (2015). Morphine disinhibits glutamatergic input to VTA dopamine neurons and promotes dopamine neuron excitation. *Elife*, *4*, <https://doi.org/10.7554/eLife.09275>
- Chieng, B., Azriel, Y., Mohammadi, S., & Christie, M. J. (2011). Distinct cellular properties of identified dopaminergic and GABAergic neurons in the mouse ventral tegmental area [published online ahead of print June 6, 2011]. *Journal of Physiology*, *589*(Pt 15), 3775–3787. <https://doi.org/10.1113/jphysiol.2011.210807>
- Dal Bo, G., St-Gelais, F., Danik, M., Williams, S., Cotton, M., & Trudeau, L.-E. (2004). Dopamine neurons in culture express VGLUT2 explaining their capacity to release glutamate at synapses in addition to dopamine. *Journal of Neurochemistry*, *88*(6), 1398–1405. <https://doi.org/10.1046/j.1471-4159.2003.02277.x>
- Fenno, L. E., Mattis, J., Ramakrishnan, C., Hyun, M., Lee, S. Y., He, M., Tucciarone, J., Selimbeyoglu, A., Berndt, A., Grosenick, L., Zalocusky, K. A. (2014). Targeting cells with single vectors using multiple-feature Boolean logic. *Nature Methods*, *11*, 763–772.
- Hnasko, T. S., Hjelmstad, G. O., Fields, H. L., & Edwards, R. H. (2012). Ventral tegmental area glutamate neurons: Electrophysiological properties and projections. *Journal of Neuroscience*, *32*, 15076–15085.
- Johnson, S. W., & North, R. A. (1992). Opioids excite dopamine neurons by hyperpolarization of local interneurons. *Journal of Neuroscience*, *12*, 483–488.
- Jones, S., & Kauer, J. A. (1999). Amphetamine depresses excitatory synaptic transmission via serotonin receptors in the ventral tegmental area. *Journal of Neuroscience*, *19*, 9780–9787.
- Khaliq, Z. M., & Bean, B. P. (2010). Pacemaking in dopaminergic ventral tegmental area neurons: depolarizing drive from background and voltage-dependent sodium conductances. *Journal of Neuroscience*, *30*(21), 7401–7413. <https://doi.org/10.1523/JNEUROSCI.0143-10.2010>
- Kudo, T., Konno, K., Uchigashima, M., Yanagawa, Y., Sora, I., Minami, M., & Watanabe, M. (2014). GABAergic neurons in the ventral tegmental area receive dual GABA/enkephalin-mediated inhibitory inputs from the bed nucleus of the stria terminalis. *European Journal of Neuroscience*, *39*(11), 1796–1809. <https://doi.org/10.1111/ejn.12503>
- Kudo, T., Uchigashima, M., Miyazaki, T., Konno, K., Yamasaki, M., Yanagawa, Y., Minami, M., & Watanabe, M. (2012). Three types of neurochemical projection from the bed nucleus of the stria terminalis to the ventral tegmental area in adult mice. *Journal of Neuroscience*, *32*(50), 18035–18046. <https://doi.org/10.1523/JNEUROSCI.4057-12.2012>
- Li, X., Qi, J., Yamaguchi, T., Wang, H. L., & Morales, M. (2013). Heterogeneous composition of dopamine neurons of the rat A10 region: Molecular evidence for diverse signaling properties [published online ahead of print August 29, 2012]. *Brain Structure and Function*, *218*(5), 1159–1176. <https://doi.org/10.1007/s00429-012-0452-z>
- Margolis, E. B., Hjelmstad, G. O., Bonci, A., & Fields, H. L. (2005). Both kappa and mu opioid agonists inhibit glutamatergic input to ventral tegmental area neurons. *Journal of Neurophysiology*, *93*, 3086–3093. <https://doi.org/10.1152/jn.00855.2004>
- Margolis, E. B., Lock, H., Hjelmstad, G. O., & Fields, H. L. (2006). The ventral tegmental area revisited: Is there an electrophysiological marker for dopaminergic neurons? *Journal of Physiology*, *577*, 907–924.
- Margolis, E. B., Toy, B., Himmels, P., Morales, M., & Fields, H. L. (2012). Identification of rat ventral tegmental area GABAergic neurons. *PLoS One*, *7*, e42365.
- Monteggia, L. M., Eisch, A. J., Tang, M. D., Kaczmarek, L. K., & Nestler, E. J. (2000). Cloning and localization of the hyperpolarization-activated cyclic nucleotide-gated channel family in rat brain. *Brain Research Molecular Brain Research*, *81*(1–2), 129–139.
- Morales, M., & Margolis, E. B. (2017). Ventral tegmental area: cellular heterogeneity, connectivity and behavior [published online ahead of print January 5, 2017]. *Nature Reviews Neuroscience*. *18*(2):73–85. <https://doi.org/10.1038/nrn.2016.165>
- Nieh, E. H., Matthews, G. A., Allsop, S. A., Presbrey, K. N., Leppla, C. A., Wichmann, R., Neve, R., Wildes, C. P., & Tye, K. M. (2015). Decoding neural circuits that control compulsive sucrose seeking. *Cell*, *160*(3), 528–541. <https://doi.org/10.1016/j.cell.2015.01.003>
- Notomi, T., & Shigemoto, R. (2004). Immunohistochemical localization of Ih channel subunits, HCN1–4, in the rat brain. *The Journal of Comparative Neurology*, *471*(3), 241–276.
- Ntamati, N. R., Creed, M., Ridouane, A., & Christian, L. (2018). Periaqueductal efferents to dopamine and GABA neurons of the VTA. *PLoS One*, *13*(1), e0190297. <https://doi.org/10.1371/journal.pone.0190297>. Published online 2018 Jan 5
- Omelchenko, N., Bell, R., & Sesack, S. R. (2009). Lateral habenula projections to dopamine and GABA neurons in the rat ventral tegmental area [published online ahead of print September 29, 2009]. *European Journal of Neuroscience*, *30*(7), 1239–1250. <https://doi.org/10.1111/j.1460-9568.2009.06924.x>
- Omelchenko, N., & Sesack, S. R. (2010). Periaqueductal gray afferents synapse onto dopamine and GABA neurons in the rat ventral tegmental area. *Journal of Neuroscience Research*, *88*(5), 981–991. <https://doi.org/10.1002/jnr.22265>
- Root, D. H., Barker, D. J., Estrin, D. J., Miranda-Barrientos, J. A., Liu, B., Zhang, S., Wang, H. L., Vautier, F., Ramakrishnan, C., Kim, Y. S., Fenno, L., Deisseroth, K., & Morales, M. (2020). Distinct Signaling by Ventral Tegmental Area Glutamate, GABA, and Combinatorial Glutamate-GABA Neurons in Motivated Behavior. *Cell Reports*, *32*(9), 108094. <https://doi.org/10.1016/j.celrep.2020.108094>
- Root, D. H., Estrin, D. J., & Morales, M. (2018). Aversion or Salience Signaling by Ventral Tegmental Area Glutamate Neurons. *iScience*, *2*(51–62), <https://doi.org/10.1016/j.isci.2018.03.008>
- Root, D. H., Mejias-Aponte, C. A., Zhang, S., Wang, H. L., Hoffman, A. F., Lupica, C. R., & Morales, M. (2014). Single rodent mesohabenular

- axons release glutamate and GABA. *Nature Neuroscience*, *17*, 1543–1551.
- Root, D. H., Zhang, S., Barker, D. J., Miranda-Barrientos, J., Liu, B., Wang, H. L., & Morales, M. (2018). Selective Brain Distribution and Distinctive Synaptic Architecture of Dual Glutamatergic-GABAergic Neurons. *Cell Reports*, *23*, 3465–3479.
- Sawamoto, K., Nakao, N., Kobayashi, K., Matsushita, N., Takahashi, H., Kakishita, K., Yamamoto, A., Yoshizaki, T., Terashima, T., Murakami, F., Itakura, T., & Okano, H. (2001). Visualization, direct isolation, and transplantation of midbrain dopaminergic neurons [published online ahead of print May 15, 2001]. *Proc Natl Acad Sci U S A*, *98*(11), 6423–6428. <https://doi.org/10.1073/pnas.111152398>
- Stamatakis, A. M., Jennings, J. H., Ung, R. L., Blair, G. A., Weinberg, R. J., Neve, R. L., Boyce, F., Mattis, J., Ramakrishnan, C., Dissersoth, K., & Stuber, G. D. (2013). A unique population of ventral tegmental area neurons inhibits the lateral habenula to promote reward. *Neuron*, *80*, 1039–1053.
- Sulzer, D., Joyce, M. P., Lin, L., Geldwert, D., Haber, S. N., Hattori, T., & Rayport, S. (1998). Dopamine Neurons Make Glutamatergic Synapses in Vitro. *The Journal of Neuroscience*, *18*(12), 4588–4602. <https://doi.org/10.1523/JNEUROSCI.18-12-04588.1998>
- Tan, K. R., Yvon, C., Turiault, M., Mirzabekov, J. J., Doehner, J., Labouèbe, G., Deisseroth, K., Tye, K. M., & Lüscher, C. (2012). GABA neurons of the VTA drive conditioned place aversion. *Neuron*, *73*, 1173–1183.
- Tateno, T., & Robinson, H. P. (2011). The mechanism of ethanol action on midbrain dopaminergic neuron firing: A dynamic-clamp study of the role of I(h) and GABAergic synaptic integration [published online ahead of print June 22, 2011]. *Journal of Neurophysiology*, *106*(4), 1901–1922. <https://doi.org/10.1152/jn.00162.2011>
- Tracy, M. E., Tesic, V., Stamenic, T. T., Joksimovic, S. M., Busquet, N., Jevtovic-Todorovic, V., & Todorovic, S. M. (2018). Ca_v3.1 isoform of T-type calcium channels supports excitability of rat and mouse ventral tegmental area neurons [published online ahead of print March 23, 2018]. *Neuropharmacology*, *135*, 343–354. <https://doi.org/10.1016/j.neuropharm.2018.03.028>
- Tritsch, N. X., Ding, J. B., & Sabatini, B. L. (2012). Dopaminergic neurons inhibit striatal output through non-canonical release of GABA [published online ahead of print October 3, 2012]. *Nature*, *490*(7419), 262–266. <https://doi.org/10.1038/nature11466>. PMID: 23034651; PMCID: PMC3944587
- van Zessen, R., Phillips, J. L., Budygin, E. A., & Stuber, G. D. (2012). Activation of VTA GABA neurons disrupts reward consumption. *Neuron*, *73*, 1184–1194.
- Wise, R. A. (2004). (2004) Dopamine, learning and motivation. *Nature Reviews Neuroscience*, *5*, 483–494.
- Woodward, T. J., Tesic, V., Stamenic, T. T., Jevtovic-Todorovic, V., & Todorovic, S. M. (2019). (2019) Pharmacological Antagonism of T-Type Calcium Channels Constrains Rebound Burst Firing in Two Distinct Subpopulations of GABA Neurons in the Rat Ventral Tegmental Area: Implications for α -Lipoic Acid. *Front Pharmacol.*, *10*, 1402. <https://doi.org/10.3389/fphar.2019.01402>. eCollection
- Yamaguchi, T., Sheen, W., & Morales, M. (2007). Glutamatergic neurons are present in the rat ventral tegmental area. *European Journal of Neuroscience*, *25*, 106–118.
- Zhang, W., Yang, H. L., Song, J. J., Chen, M., Dong, Y., Lai, B., Yu, Y. G., Ma, L., & Zheng, P. (2015). DAMGO depresses inhibitory synaptic transmission via different downstream pathways of μ opioid receptors in ventral tegmental area and periaqueductal gray [published online ahead of print June 3, 2015]. *Neuroscience*, *301*, 144–154. <https://doi.org/10.1016/j.neuroscience.2015.05.077>
- Zhou, Z., Liu, X., Chen, S., Zhang, Z., Liu, Y., Montardy, Q., Tang, Y., Wei, P., Liu, N., Li, L., Song, R., Lai, J., He, X., Chen, C., Bi, G., Feng, G., Xu, F., & Wang, L. (2019). A VTA GABAergic Neural Circuit Mediates Visually Evoked Innate Defensive Responses [published online ahead of print June 12, 2019]. *Neuron*, *103*(3), 473–488.e6. <https://doi.org/10.1016/j.neuron.2019.05.027>

How to cite this article: Miranda-Barrientos J, Chambers I, Mongia S, et al. Ventral tegmental area GABA, glutamate, and glutamate-GABA neurons are heterogeneous in their electrophysiological and pharmacological properties. *Eur J Neurosci.* 2021;54:4061–4084. <https://doi.org/10.1111/ejn.15156>